Chapter 12

Surface Modes in Small Particles

There is a class of electromagnetic modes in small particles, called *surface modes*, which give rise to interesting—perhaps puzzling at first sight—absorption spectra: small-particle absorption spectra can have features where none exist in the bulk and several features where only a single absorption band exists in the bulk. Particle shape and the variation of the dielectric function determine the number, position, and width of such features, which are manifestations of surface modes. Despite their dominant influence on absorption and scattering, and the ease with which they emerge from simple theory, surface modes have received little attention, particularly from applied scientists.

The extinction curves for magnesium oxide particles (Fig. 11.2) and aluminum particles (Fig. 11.4) show the dominance of surface modes. The strong extinction by MgO particles near 0.07 eV($\sim$ 17 μm) is a surface mode associated with lattice vibrations. Even more striking is the extinction feature in aluminum that dominates the ultraviolet region near 8 eV: no corresponding feature exists in the bulk solid. Magnesium oxide and aluminum particles will be treated in more detail, both theoretically and experimentally, in this chapter.

In Sections 12.1 and 12.2 we discuss the theory of surface modes in spherical and nonspherical particles, respectively; in Sections 12.3 and 12.4 comparisons between theory and experiment are given, first for insulators and then for metals and metal-like materials.

There are several persistent misconceptions about the interaction of light with particles small enough to be described by Rayleigh theory. One is that they are very "inefficient" absorbers and scatterers of light. By any measure of efficiency, including the conventional efficiency Q (a somewhat unusual efficiency as it is not restricted to be less than 1), the small particles discussed in this chapter are very efficient. $Q_{\rm abs}$ is often much greater than 1, and small particles are, per unit mass, among the most efficient of absorbing materials. Another common misconception is that if a particle is small compared with the wavelength, an electromagnetic wave does not probe the details of its structure and, consequently, shape does not appreciably affect its absorption spectrum:

small particles obediently follow in the footsteps of the parent material. In fact, one of the most interesting aspects of small particles is that they can exhibit absorption features that are totally dominated by shape and that bear little resemblance to those of the bulk material. When first confronted with intense shape-dependent absorption in very small particles there is an unfortunate tendency to assume that bulk dielectric functions have become inapplicable, perhaps because of the importance of quantum-level spacings. We emphasize, however, that these effects can usually be explained satisfactorily with classical electromagnetic theory (indeed, classical electrostatics!) and bulk optical constants.

12.1 SURFACE MODES IN SMALL SPHERES

The conditions for the vanishing of the denominators of the scattering coefficients a_n and b_n for a homogeneous sphere are (4.54) and (4.55). We now consider these conditions in the limit of vanishingly small x. From the series expansions (5.1) and (5.2) of the spherical Bessel functions of order n, together with a bit of algebra, we can show that the denominator of a_n vanishes in the limit $x \to 0$ (finite $|m|$) provided that

$$m^2 = -\frac{n+1}{n}, \qquad n = 1, 2, \ldots \tag{12.1}$$

where we have taken the sphere to be nonmagnetic. In the limit $x \to 0$ there is no solution to (4.55), the condition that the denominator of b_n vanish, for any n. At frequencies where (12.1) is satisfied, the corresponding scattering coefficient a_n is infinite. These frequencies are complex and, consequently, the associated normal modes are said to be *virtual*. Nevertheless, at real frequencies close to these complex frequencies, the scattering coefficients will be large. If (12.1) is approximately satisfied at some frequency, there will be a maximum, or resonance, in the cross sections. We shall refer to the normal modes (i.e., the vector spherical harmonics) associated with these frequencies as *surface modes*; they are characterized by internal electric fields with no radial nodes. The radial variation of the radial component of the electric field inside the sphere for a given normal mode is, from (4.40), (4.50), and (5.1),

$$E_{1r} \propto \left(\mathbf{N}_{e1n}^{(1)}\right)_r \propto r^{n-1} \qquad (x, |m|x \ll 1). \tag{12.2}$$

The greater the order of the normal mode, the more the field is localized near the surface of the sphere, hence the designation surface modes. The lowest-order mode ($n = 1$) is uniform throughout the sphere, and this mode is sometimes called the *mode of uniform polarization*.

For sufficiently small spheres, a_1 will be the dominant coefficient; for $n = 1$ the condition (12.1) is

$$m^2 = -2. \tag{12.3}$$

If, for the moment, we take the sphere to be in free space, then (12.3) in component form becomes

$$n^2 - k^2 = -2; \qquad 2nk = 0, \tag{12.4}$$

where $n + ik$ is the complex refractive index of the particle. The solution to (12.4) is

$$n = 0; \qquad k = \sqrt{2}. \tag{12.5}$$

The conditions (12.5) have been stumbled upon from time to time and then dismissed as "unphysical": n cannot be 0! But the reader who has faithfully waded through Chapters 9 and 10 should by now be somewhat hardened to refractive indices less than 1—or even 0. Indeed, one of our objectives in Chapter 9 was to clear the way for the introduction of (12.5), knowing full well that it is often unpalatable. Prejudices about what the dielectric function can or cannot be are not nearly so deeply rooted as those surrounding the refractive index; thus, (12.3) can be cast in a more palatable form in terms of the complex dielectric function of the particle $\epsilon = \epsilon' + i\epsilon''$:

$$\epsilon = -2\epsilon_m, \tag{12.6}$$

where ϵ_m is the dielectric function of the surrounding medium (assumed to be nonabsorbing). The solution to (12.6) is

$$\epsilon' = -2\epsilon_m; \qquad \epsilon'' = 0. \tag{12.7}$$

We shall call the frequency at which $\epsilon' = -2\epsilon_m$ and $\epsilon'' \simeq 0$ the *Fröhlich frequency* ω_F; the corresponding normal mode—the mode of uniform polarization—is sometimes called the *Fröhlich mode*. In his excellent book on dielectrics, Fröhlich (1949) obtained an expression for the frequency of polarization oscillation due to lattice vibrations in small dielectric crystals. His expression, based on a one-oscillator Lorentz model, is similar to (12.20). The frequency that Fröhlich derived occurs where $\epsilon' = -2\epsilon_m$. Although he did not explicitly point out this condition, the frequency at which (12.6) is satisfied has generally become known as the Fröhlich frequency. The oscillation mode associated with it, which is in fact the lowest-order surface mode, has likewise become known as the Fröhlich mode. Whether or not Fröhlich's name should be attached to these quantities could be debated; we shall not do so, however. It is sufficient for us to have convenient labels without worrying about completely justifying them.

The condition (12.6) has on occasion been attributed to Mie, presumably because it can be obtained from the Mie theory. But it is sobering to realize that it follows from simple electrostatics. For we showed in Section 5.2 that the absorption efficiency in the electrostatics approximation is

$$Q_{\text{abs}} = 4x \operatorname{Im}\left\{ \frac{\epsilon - \epsilon_m}{\epsilon + 2\epsilon_m} \right\}, \tag{12.8}$$

from which (12.6) follows almost trivially. (We have omitted the subscript 1 from ϵ for convenience; it will be reintroduced when we discuss coated particles.) Prediction of a resonance in the cross sections at the frequency where $\epsilon = -2\epsilon_m$ underscores our assertion at the beginning of Chapter 9 that it is often more enlightening to express various quantities in terms of the dielectric function rather than the refractive index. If we write (12.8) in terms of the relative refractive index m,

$$Q_{\text{abs}} = 4x \operatorname{Im}\left\{\frac{m^2 - 1}{m^2 + 2}\right\},$$

then the resonance is almost certain not to be noticed: there is a deep psychological resistance to looking upon the square of the refractive index as anything other than an inherently positive number. So we encourage a kind of bilingualism when considering the optics of small particles.

The origin of the misconception that the absorption spectrum of particles in the Rayleigh limit is not appreciably different from that of the bulk parent material is easy to trace. Again, for convenience, let us take the particles to be in free space. In Chapter 3 we defined the volume attenuation coefficient α_v as the extinction cross section per unit particle volume; if absorption dominates extinction, then α_v for a sphere is $3Q_{\text{abs}}/4a$, where a is the radius. If we assume that $n \gg k$, which is true for most insulating solids at *visible* wavelengths, then

$$\alpha_v \simeq \frac{9n}{(n^2 + 2)^2}\alpha \qquad (n \gg k), \tag{12.9}$$

where $\alpha = 4\pi k/\lambda$ is the bulk absorption coefficient. The factor multiplying α in (12.9) does not vary greatly over spectral regions in which n does not vary greatly and in many instances is not much different from 1. But this is not always true; in particular, n can vary greatly in the negative ϵ' region where, moreover, the assumption that k is much less than n, which is necessary for the validity of (12.9), completely breaks down. Thus, (12.9) is not always a reliable guide to spectral effects in small spheres (or, indeed, small particles of any shape); there will be many illustrations of this in succeeding paragraphs.

Let us return now to the general expression (12.8) for absorption by small spheres and write it as a function of ϵ' and ϵ'':

$$Q_{\text{abs}} = 12x\frac{\epsilon_m\epsilon''}{(\epsilon' + 2\epsilon_m)^2 + \epsilon''^2}. \tag{12.10}$$

The absorption efficiency at the Fröhlich frequency is therefore

$$Q_{\text{abs}}(\omega_F) = \frac{12x\epsilon_m}{\epsilon''(\omega_F)}, \tag{12.11}$$

which runs completely counter to intuition: the maximum absorption is *inversely* proportional to the absorptive part of the complex dielectric function. Note that although x is restricted to small values, say $x < 0.1$, Q_{abs} is not necessarily small at the Fröhlich frequency. For example, if x is 0.1 and $\epsilon''(\omega_F)/\epsilon_m$ is 0.1 (and there is no physical reason why it cannot take on this or even smaller values), then $Q_{abs} = 12$!

We tacitly assumed in the preceding paragraph that the absorption maximum in the region where ϵ' is negative occurs at the Fröhlich frequency. Although this is not strictly correct, the Fröhlich frequency is usually approximately equal to the frequency of maximum absorption; the precise position of the maximum depends on the behavior of the dielectric function and can be determined only by detailed calculations. This is analogous to the position of absorption peaks in the bulk material: we usually assume that such peaks occur at the maxima of ϵ'', whereas this is only approximately correct.

12.1.1 The Effect of Finite Size on the Fröhlich Frequency

Equation (12.6) is strictly valid only in the limit of vanishingly small x. We can obtain a better approximate condition for small but finite-sized particles by retaining more terms in the series expansions (5.1) and (5.2). The condition that the denominator of a_1 vanish is, from (4.54),

$$m\psi_1(mx)\xi_1'(x) - \xi_1(x)\psi_1'(mx) = 0. \tag{12.12}$$

If ψ_1 is expanded to terms of order x^4 and ξ_1 to terms of order x, then (12.12) correct to terms of order x^2 is

$$\epsilon = -\left(2 + \tfrac{12}{5}x^2\right)\epsilon_m. \tag{12.13}$$

For small x, this is not appreciably different from (12.6). However, (12.13) gives us an indication of how the Fröhlich frequency shifts as the size of the sphere increases. If in the neighborhood of the frequency where $\epsilon = -2\epsilon_m$ the real part of the dielectric function is an increasing function of frequency (this will almost always be so), an increase in particle size shifts the Fröhlich frequency to lower values (i.e., to longer wavelengths).

12.1.2 The Effect of a Coating

In the preceding paragraphs we considered a homogeneous sphere. Let us now examine what happens when a homogeneous core sphere is uniformly coated with a mantle of different composition. Again, the condition for excitation of the first-order surface mode can be obtained from electrostatics. In Section 5.4 we derived an expression for the polarizability of a small coated sphere; the condition for excitation of the Fröhlich mode follows by setting the denominator of (5.36) equal to zero:

$$(\epsilon_2 + 2\epsilon_m)(\epsilon_1 + 2\epsilon_2) + f(2\epsilon_2 - 2\epsilon_m)(\epsilon_1 - \epsilon_2) = 0, \tag{12.14}$$

where ϵ_1 and ϵ_2 are the dielectric functions of core and mantle, respectively, and f is the fraction of the total particle volume occupied by the core. If we take the dielectric function ϵ_m of the surrounding medium to be 1, then (12.14) becomes

$$\epsilon_1 = -2\epsilon_2\left[\frac{\epsilon_2(1-f)+(2+f)}{\epsilon_2(2f+1)+2(1-f)}\right]. \tag{12.15}$$

As a check on (12.15) we note that $\epsilon_1 = -2$ when $f = 1$, as required. If the core volume is small compared with that of the mantle ($f \ll 1$), then (12.15) becomes $\epsilon_1 \simeq -2\epsilon_2$, which is the Fröhlich mode condition for a homogeneous sphere with dielectric function ϵ_1 in a medium with dielectric function ϵ_2 (this is not a particularly startling result). Thus, the effect of coating a small, homogeneous sphere is to shift its Fröhlich frequency; the magnitude of this shift depends on the behavior of ϵ_1 as well as the kind and amount of coating.

12.1.3 Fröhlich Modes of Voids and Bubbles

In previous chapters we have always taken particles to be in a nonabsorbing medium. We now briefly remove this restriction. The notion of extinction by particles in an absorbing medium is not devoid of controversy: more than one interpretation is possible. But Bohren and Gilra (1979) showed that if the extinction cross section is interpreted as the reduction in area of a detector because of the presence of a particle [see Section 3.4, particularly the development leading up to (3.34)], then the optical theorem for a spherical particle in an absorbing medium is formally similar to that for a nonabsorbing medium:

$$C_{\text{ext}} = 4\pi \operatorname{Re}\left[\frac{S(0°)}{k^2}\right], \tag{12.16}$$

where the wave number k is now *complex*. For a nonabsorbing medium k is real and may be taken outside the brackets in (12.16). As before, we may *define* the extinction efficiency Q_{ext} as $C_{\text{ext}}/\pi a^2$, which in the small-particle limit is

$$Q_{\text{ext}} = 4\operatorname{Im}\left\{\frac{x(\epsilon-\epsilon_m)}{\epsilon+2\epsilon_m}\right\}. \tag{12.17}$$

Note that the size parameter x for a sphere in an absorbing medium is complex.

Consider now a spherical *void* ($\epsilon = 1$) in an otherwise homogeneous medium. Light is not absorbed by such a void, but it can influence the absorption of light in the surrounding medium. The condition for a resonance in the extinction efficiency of a small spherical void follows readily from (12.17):

$$\epsilon_m = -\tfrac{1}{2}. \tag{12.18}$$

The resonance condition for a hollow sphere, or *bubble*, in air is, from (12.14),

$$(\epsilon + 2)(1 + 2\epsilon) + f(2\epsilon - 2)(1 - \epsilon) = 0, \tag{12.19}$$

where ϵ is the dielectric function of the solid part of the bubble. There are two roots to (12.19):

$$\epsilon_+ = \frac{-(5 + 4f) + 3\sqrt{1 + 8f}}{4 - 4f}, \qquad \epsilon_- = \frac{-(5 + 4f) - 3\sqrt{1 + 8f}}{4 - 4f}.$$

If f is small (a nearly solid bubble), the two roots are approximately $\epsilon_+ = -\frac{1}{2}$ and $\epsilon_- = -2$; these are the resonance conditions for a spherical void in a medium with dielectric function ϵ and a solid sphere with dielectric function ϵ in free space, respectively. As f is increased ϵ_+ increases monotonically and ϵ_- decreases monotonically, where $\lim_{f\to 1} \epsilon_+ = 0$ and $\lim_{f\to 1} \epsilon_- = -\infty$. (Of course, when $f = 1$, the bubble bursts!)

Up to this point we have considered only the conditions for resonances in the cross sections of small spherical particles of various kinds; we have said nothing quantitative about their strengths and the frequencies at which they might occur other than brief introductory remarks about ionic crystals in the infrared and metals in the ultraviolet. To determine if a resonance is realizable, where it occurs, and its strength, we need to know how the dielectric function varies with frequency. Therefore, in the following sections we shall examine some of the preceding resonance conditions in the light of simple, but realistic, dielectric functions.

12.1.4 Crystals with Simple Vibrational Modes

Detailed calculations of surface modes in small spherical particles are best carried out using the exact theory and measured optical constants. Even though simple models may fit measured data reasonably well, there can be considerable differences between calculations based on model and measured optical constants. This has been stressed by Hunt et al. (1973), who illustrated their point with NiO. Nevertheless, the usefulness of back-of-the-envelope calculations is not to be gainsaid provided their limitations are kept firmly in mind. Cross-section resonances for spheres are sharp and, consequently, are often missed in calculations done in a state of ignorance about their existence; it is wise to chart the approximate position of resonances before beginning a series of calculations. In the following paragraphs, therefore, we examine the consequences of (12.6) for crystals that are well described by the simple one-oscillator model of Section 9.1. We shall sometimes loosely refer to such crystals as "ionic," which is not strictly correct. The reason for this terminology is that strongly ionic crystals have been given prominence in work on lattice vibrational modes. But ionic particles are not the only ones that can

support surface modes. Indeed, an ionic crystal is a limiting case, an idealization, in which bonding is entirely Coulombic and covalent bonding is negligible.

If we ignore damping, the Fröhlich frequency follows readily from (12.6), (9.21), and (9.23):

$$\omega_F^2 = \omega_t^2 \left(\frac{\epsilon_{0v} + 2\epsilon_m}{\epsilon_{0e} + 2\epsilon_m} \right). \tag{12.20}$$

A consequence of (9.23) and (9.24) is that $\omega_t < \omega_F < \omega_l$. This is no more than a statement that (12.6) is satisfied only in the region where ϵ' is negative, which, for simple one-oscillator materials, lies between ω_t and ω_l; we shall call this the surface mode region.

Laboratory measurements of extinction spectra are often done with particles suspended in some nonvacuous medium. It is usually taken for granted that features in such spectra are insensitive to this medium provided that it is weakly absorbing, but in the surface mode region this assumption can be greatly in error. For if we differentiate (12.20) with respect to ϵ_m, which we take to be greater than or equal to 1, then $d\omega_F/d\epsilon_m < 0$; in going from air to some nonvacuous medium, the Fröhlich frequency shifts to a lower value. Note that the magnitude of this shift depends on the width of the surface mode region: it can *at most* be $\omega_l - \omega_t$. This is just one example of an important general rule about surface modes: their characteristics strongly depend on how the dielectric function varies with frequency.

We noted in Section 9.1 that for a one-oscillator model, $\epsilon''(\omega)$ falls to one-half its maximum value $\epsilon''(\omega_t)$ at $\omega = \omega_t \pm \gamma/2$ provided that $\gamma/\omega_t \ll 1$. Under the same condition on γ/ω_t [see (12.33)] the half-width of the sphere absorption spectrum (12.10) is also γ. That is, the *width* of the absorption band is preserved in going from the bulk to particulate states, although the *position* of the band can be appreciably shifted.

We now pause briefly in the theoretical discussion to consider a specific example, silicon carbide, the infrared optical constants of which are given to good approximation by a one-oscillator model (Fig. 9.6). Extinction efficiencies for small silicon carbide spheres in air calculated from Mie theory and the parameters of Fig. 9.6 are shown in Fig. 12.1. For the 0.1-μm-radius sphere, which is sufficiently small that Rayleigh theory is adequate, the single extinction feature at 930 cm^{-1} is the Fröhlich mode, or lowest-order surface mode; its position is very near that predicted by (12.20). The frequency at which absorption is a maximum is appreciably shifted from what it would be in thin films, the transverse optic mode frequency $\omega_t = 793$ cm^{-1}. The small-particle extinction efficiency at ω_F is orders of magnitude greater than that at ω_t, which does not even show on the linear plot. As the size is increased, the surface mode peak shifts slightly to lower frequencies, in accordance with (12.13), and broadens as higher-order surface modes, which are not resolved on this plot, are excited. Simultaneously, an increasingly complicated series of modes

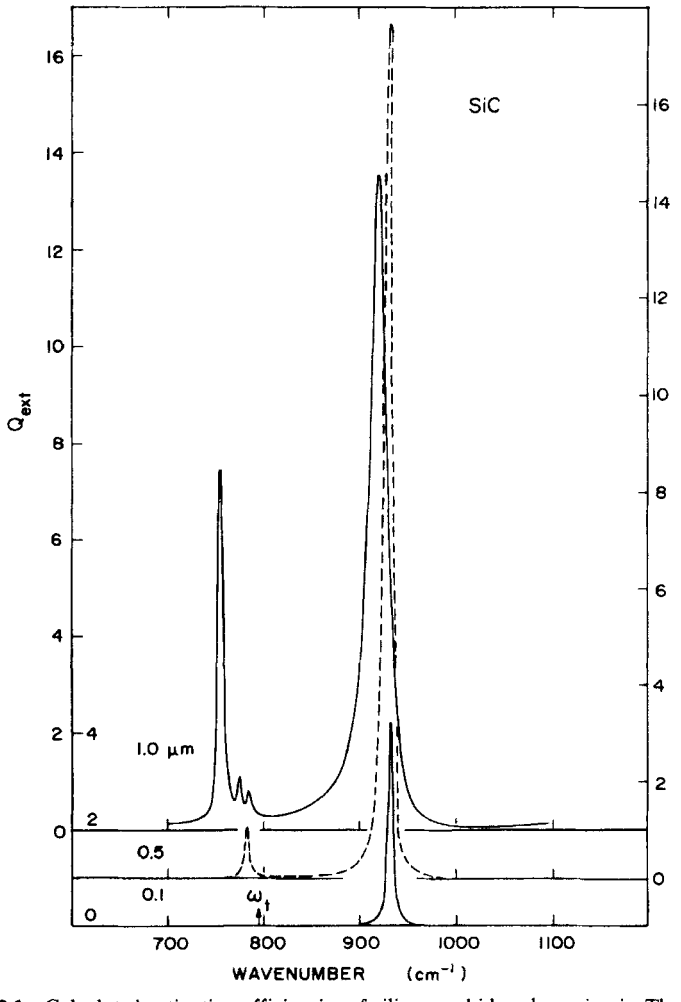

Figure 12.1 Calculated extinction efficiencies of silicon carbide spheres in air. The wave number denotes the inverse of the wavelength.

appears just below ω_t. These modes are of the same nature as the ripple structure modes discussed in Chapter 11. They appear at rather small size parameters in this instance because the refractive index rises to very large values just below ω_t (Fig. 9.6). Fuchs and Kliewer (1968) have given a detailed discussion of the positions and widths of these modes, which they call "low-frequency modes." It is worth noting again that the extinction efficiency Q_{ext} can be much greater than 1 in the surface mode region even for spheres small compared with the wavelength.

Extinction spectra for a 0.1-μm-radius SiC sphere in potassium bromide ($\epsilon_m = 2.33$) and in air ($\epsilon_m = 1$) are shown in Fig. 12.2. The Fröhlich mode

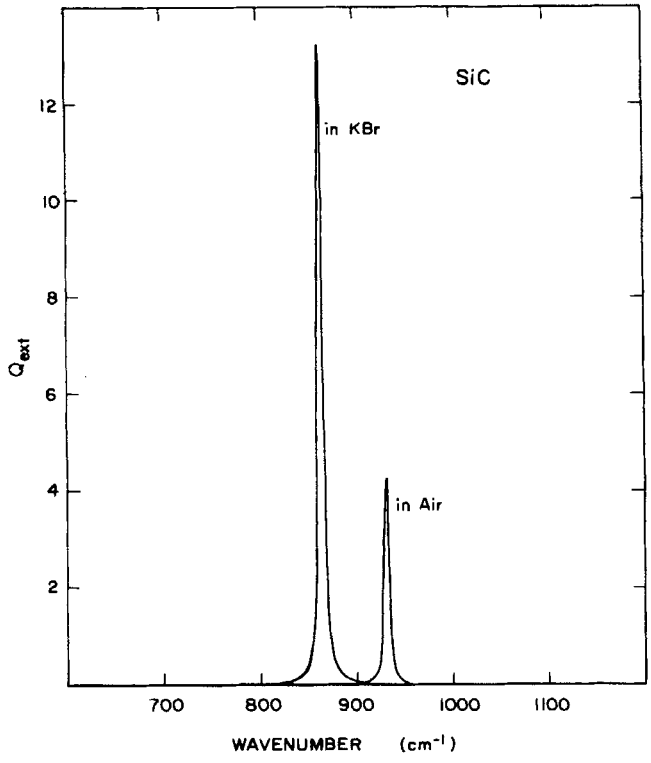

Figure 12.2 Calculated extinction efficiencies of a silicon carbide sphere (0.1 μm) in air and in potassium bromide.

shifts to a lower frequency in going from air to KBr, in agreement with (12.20). Note also that the extinction efficiency at the Fröhlich frequency is greater for the particle in a KBr matrix than in air even though KBr is nonabsorbing over the SiC surface mode region.

A number of experiments over the past 10 years have qualitatively confirmed that the general aspects of absorption by small ionic particles are in accord with the preceding discussion for spheres. In particular, the dominant absorption peak is shifted toward higher frequencies in going from bulk to particulate states and there is a predictable shift depending on the surrounding medium. Some notable examples are the alkali halides KCl, NaCl, and KBr (Martin, 1969, 1970, 1971; Bryksin et al., 1971), MgO (Genzel and Martin, 1972, 1973), and UO_2 and ThO_2 (Axe and Pettit, 1966). Notably lacking in the comparison between theory and experiment has been agreement about the width and strength of absorption bands. To understand these discrepancies requires that we consider the effect of departures from sphericity; this will be undertaken in Section 12.2 as a prelude to further discussion of vibrational modes in insulators.

12.1.5 Simple Metals

We showed in the preceding section that for solids with strong vibrational bands the position of features in absorption spectra can be shifted appreciably in going from the bulk to particulate states. Metallic particles can deviate even more markedly from the behavior of the bulk parent material: they can have absorption features over broad frequency regions where *none* appear in the bulk. For a simple metal—one that is well described by the Drude formula (9.26)—the imaginary part of the dielectric function has no maximum: it merely decreases monotonically with increasing frequency. But there will be a peak in the absorption cross section of a small spherical particle of such a metal near the frequency ω_F where $\epsilon = -2\epsilon_m$. If $\gamma^2 \ll \omega_p^2$, it follows from (9.27) that

$$\omega_F = \frac{\omega_p}{\sqrt{1 + 2\epsilon_m}}. \tag{12.21}$$

In air $\epsilon_m = 1$ and (12.21) reduces to

$$\omega_F = \frac{\omega_p}{\sqrt{3}}. \tag{12.22}$$

Unlike ionic materials, the negative ϵ' region for a simple metal is not confined to a relatively narrow band of frequencies: the surface mode region extends from ω_p down to zero frequency. As a consequence, metallic particles can be richer in surface modes than ionic particles. This will become apparent in Section 12.2 when we discuss the effect of shape on surface modes; for the moment, we content ourselves with spheres.

Following (9.27) we discussed the physical interpretation of the plasma frequency for a simple metal and introduced the concept of a plasmon, a quantized plasma oscillation. It may help our understanding of the physics of surface modes in small particles and the terminology sometimes encountered in their description if we expand that discussion.

It was tacitly assumed in Chapter 9 that the plasma was unbounded; that is, we had in mind *bulk* plasmons. But because of the long-range nature of the organizing forces in a plasma oscillation, it is reasonable to expect that for a sufficiently small system, the electrons will sense the presence of the boundaries and modify their collective behavior accordingly. Indeed, following hard on the heels of the acceptance of bulk plasmons in metals came the realization that *surface plasmons* were possible in thin films (Ritchie, 1957; Stern and Ferrell, 1960). Whereas the energy of a bulk plasmon is $\hbar\omega_p$, that of a surface plasmon in a thin film (in air) is $\hbar\omega_p/\sqrt{2}$. The next member of this family of plasmons is the surface plasmon in a sphere (in air) with energy $\hbar\omega_p/\sqrt{3}$ [see (12.22)]. Thus, surface modes in small metallic particles are often called *surface plasmons*. All of this illustrates a general rule, which we can state but not prove: if there is an interesting effect in a thin film, there will be a corresponding effect,

albeit with possibly a few new twists, in small particles. Both are examples of systems with at least one small dimension.

Ions in the lattice of a solid can also partake in a collective oscillation which, when quantized, is called a *phonon*. Again, as with plasmons, the presence of a boundary can modify the characteristics of such lattice vibrations. Thus, the infrared surface modes that we discussed previously are sometimes called *surface phonons*. Such surface phonons in ionic crystals have been clearly discussed in a landmark paper by Ruppin and Englman (1970), who distinguish between *polariton* and pure phonon modes. In the classical language of Chapter 4 a polariton mode is merely a normal mode where no restriction is made on the size of the sphere; pure phonon modes come about when the sphere is sufficiently small that retardation effects can be neglected. In the language of elementary excitations a polariton is a kind of hybrid excitation that exhibits mixed photon and phonon behavior.

The choice of quantum-mechanical or classical language to describe surface modes in small particles is dictated more by taste than by necessity. However, there is an unfortunate tendency among physicists to consider that "quantum mechanics is intrinsically better than classical mechanics, and that classical mechanics is something real physicists ought to grow out of"; we agree with Pippard (1978, p. 3) that this is a "disputable proposition." Indeed, much mischief has been done—and is still being done—by incorrectly applying quantum theory to "explain" the strange optical behavior of small particles. Surface modes in small particles are adequately and economically described in their essentials by simple classical theories. Even, however, in the classical description, quantum mechanics is lurking unobtrusively in the background; but it has all been rolled up into a handy, ready-to-use form: the dielectric function, which contains all the required information about the collective as well as the individual particle excitations. The effect of a boundary, which is, after all, a macroscopic concept, is taken care of by classical electromagnetic theory.

We must again emphasize, even more strongly than we did at the beginning of this chapter, that surface plasmons and surface phonons are not examples of the failure of the bulk dielectric function to be applicable to small particles. Down to surprisingly small sizes—exactly how small is best stated in specific examples, as in Sections 12.3 and 12.4—the dielectric function of a particle is the same as that of the bulk parent material. But this dielectric function, which is the repository of information about elementary excitations, manifests itself in different ways depending on the size and shape of the system.

12.1.6 Limitation of the Mean Free Path

There is one clear exception to the rule that bulk dielectric functions tend to be applicable to very small particles: in metal particles smaller than the mean free path of conduction electrons in the bulk metal, the mean free path can be dominated by collisions with the particle boundary. This effect has been

invoked by many authors, including Doyle (1958), Doremus (1964), Kreibig and von Fragstein (1969), Kreibig (1974), and Granqvist and Hunderi (1977).

The dielectric function of a metal can be decomposed into a free-electron term and an interband, or bound-electron term, as was done for silver in Fig. 9.12. This separation of terms is important in the mean free path limitation because only the free-electron term is modified. For metals such as gold and copper there is a large interband contribution near the Fröhlich mode frequency, but for metals such as silver and aluminum the free-electron term dominates. A good discussion of the mean free path limitation has been given by Kreibig (1974), who applied his results to interpreting absorption by small silver particles. The basic idea is simple: the damping constant in the Drude theory, which is the inverse of the collision time for conduction electrons, is increased because of additional collisions with the boundary of the particle. Under the assumption that the electrons are diffusely reflected at the boundary, γ can be written

$$\gamma = \gamma_{\text{bulk}} + \frac{v_F}{L},$$

where γ_{bulk} is the bulk metal damping constant, v_F is the electron velocity at the Fermi surface, and L is the effective mean free path for collisions with the boundary. Kreibig used $L = 4a/3$ for a sphere of radius a, although there is slight disagreement among various authors about the constant of proportionality between L and a.

Near the plasma frequency in metals $\omega^2 \gg \gamma^2$; therefore, to good approximation, the imaginary part of the Drude dielectric function (9.26) is

$$\epsilon''(\omega, a) = \frac{\omega_p^2}{\omega^3}\gamma = \frac{\omega_p^2}{\omega^3}\left(\gamma_{\text{bulk}} + \frac{3v_F}{4a}\right)$$

$$= \epsilon''_{\text{bulk}} + \frac{3}{4}\frac{\omega_p^2}{\omega^3}\frac{v_F}{a}. \tag{12.23}$$

Although the effect of the mean free path limitation on the real part of the dielectric function is slight, the effect on the imaginary part is often substantial. For small silver particles Kreibig (1974) found that ϵ'' near the Fröhlich frequency is given by

$$\epsilon'' = 0.23 + \frac{26.4}{a},$$

where a is in angstroms. Thus, ϵ'' is enhanced by more than 10% for particles of radius 1000 Å, and for a radius of about 115 Å, ϵ'' is twice the bulk value. The effect of the decreased mean free path is to increase the width and lower the peak height of the surface plasmon absorption. A combination of Mie

theory and the free-electron contribution to the dielectric function suitably modified to include the mean free path limitation gives good agreement with experiments in which the metal particles are spherical and well isolated from one another.

12.1.7 Surface Modes in Small Aluminum Spheres

As an example of extinction by spherical particles in the surface plasmon region, Fig. 12.3 shows calculated results for aluminum spheres using optical constants from the Drude model taking into account the variation of the mean free path with radius by means of (12.23). Figure 9.11 and the attendant discussion have shown that the free-electron model accurately represents the bulk dielectric function of aluminum in the ultraviolet. In contrast with the Q_{ext} plot for SiC (Fig. 12.1), we now plot volume-normalized extinction. Because this measure of extinction is independent of radius in the small size

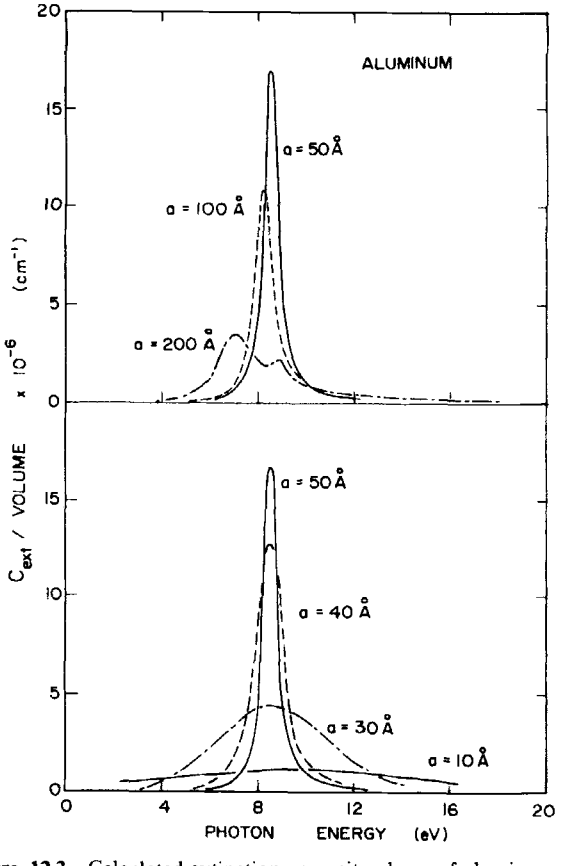

Figure 12.3 Calculated extinction per unit volume of aluminum spheres.

limit deviations from Rayleigh theory are clearly evident. The upper curve of Fig. 12.3 shows the shift of the Fröhlich mode toward lower energies as the size increases (12.13). A higher-order surface mode is also obvious in the curve for the 200-Å particle. The net result of increasing size is thus a shift of the maximum toward lower energies, broadening of the band, and a decrease in volume-normalized extinction. The lower part of the figure shows calculated results for radii smaller than 50 Å, where the mean free path limitation becomes an appreciable effect. Increased damping in the Drude formula (9.26) gives rise to an increased width of the dominant, lowest-order surface mode; at the same time the peak height is reduced. Both the excitation of higher-order surface modes with increasing size and greater damping for very small particles have been verified experimentally; this will be discussed in Section 12.4.

12.1.8 Field Lines of the Poynting Vector

Small spheres can absorb more than the light incident on them. The truth of this assertion follows from simple calculations using (12.11). But analytical proofs have less force, to some minds at least, than geometrical proofs. For this reason, therefore, we consider the interaction of light with a small sphere in a way which, as far as we know, has not been done before. The result is not new knowledge but rather new evidence supporting and firmly implanting in our minds what we already know.

We showed in Section 3.3 that the total Poynting vector $\mathbf{S}$ in the region surrounding an arbitrary particle can be written as the sum of three terms:

$$\mathbf{S} = \mathbf{S}_i + \mathbf{S}_s + \mathbf{S}_{\text{ext}}.$$

$\mathbf{S}_i$ is the Poynting vector of the incident field and $\mathbf{S}_s$ that of the scattered field; we may interpret $\mathbf{S}_{\text{ext}}$ as the term that arises because of interaction between the incident and scattered fields. Of greater interest here, however, is the flow of electromagnetic energy exclusive of that scattered. Thus, the Poynting vector under consideration (normalized by I_i, the magnitude of $\mathbf{S}_i$) is

$$\mathbf{A} = \frac{\mathbf{S}_i + \mathbf{S}_{\text{ext}}}{I_i}.$$

Were it not for the particle, of course, $\mathbf{A}$ would just be a unit vector parallel to the direction of propagation of the incident plane wave, and the field lines would be parallel lines. At sufficiently large distances from the particle the field lines are nearly parallel, but close to it they are distorted. It is the nature of this distortion in the neighborhood of a small sphere and its relation to the optical properties of the sphere that we now wish to investigate.

If the incident wave is x-polarized, the ϕ-component of $\mathbf{A}$ is zero in the xz plane ($\phi = 0$). In this plane, therefore, the field lines are solutions to the differential equation

$$\frac{dr}{d\theta} = \frac{rA_r}{A_\theta}. \tag{12.24}$$

For a sufficiently small sphere, a_1 is the dominant scattering coefficient in the series (4.45) and is given by (5.4). All the ingredients are at hand, therefore, for writing (12.24) in explicit form, a laborious task the details of which are best omitted; the result is

$$\frac{d\rho}{d\theta} = -\rho\frac{\cos\theta}{\sin\theta} \times \frac{\left[\rho^3 + \{(x^2\rho^2\cos\theta + x^2\rho^2 - 1)(K_r\cos\xi + K_i\sin\xi) + (x\rho\cos\theta + x\rho)(K_r\sin\xi - K_i\cos\xi)\}\right]}{\left[\rho^3 + \{(x^2\rho^2\cos\theta + 2)(K_r\cos\xi + K_i\sin\xi) + (x\rho\cos\theta - 2x\rho)(K_r\sin\xi - K_i\cos\xi)\}\right]}, \quad (12.25)$$

where $K = K_r + iK_i = (\epsilon - 1)/(\epsilon + 2)$, $\xi = x\rho(\cos\theta - 1)$, and $\rho = r/a$. Subject to restrictions on the size of the sphere, (12.25) is completely general: it gives the field lines of the Poynting vector right up to the boundary of the sphere.

This equation was solved numerically with a fourth-order Runge–Kutta scheme. It was usually more convenient to recast (12.25) as a differential equation in the rectangular Cartesian coordinates; sometimes, however, the advantage was tipped in favor of the polar coordinates. The results shown in Fig. 12.4 were obtained with a mixture of the two approaches.

At a photon energy of about 8.8 eV—the surface plasmon energy—the real part of the dielectric function of aluminum is -2; the corresponding imaginary part is about 0.2. It follows from (12.11), therefore, that the absorption efficiency of a small aluminum sphere (in air) with size parameter 0.3 is about 18: such a sphere presents to incident photons a target area 18 times greater than its geometrical cross-sectional area. More palpable evidence of the sphere's great size in this instance is provided by Fig. 12.4*a*, which shows the field lines of **A** in the region surrounding the sphere. Note the strong convergence of field lines near the sphere; light that, according to geometrical optics, would have passed the sphere without impediment, is deflected toward it.

An absorption cross section 18 times greater than the geometrical cross section implies that the absorption radius—to coin a term—is about 4.2 times greater than the geometrical radius. This follows from the analytical expression (12.11), but it should also emerge from purely geometrical reasoning. And indeed it does: note in Fig. 12.4*a* that those field lines extending to about 3.9 times the particle radius converge onto the particle.

At energies on either side of 8.8 eV a small aluminum sphere presents a much smaller target to incident photons. At 5 eV, for example, the absorption efficiency of a sphere with $x = 0.3$ is about 0.1; as far as absorption is concerned, the sphere is much smaller than its geometrical cross-sectional area. The field lines of the Poynting vector, shown in Fig. 12.4*b*, are what are to be

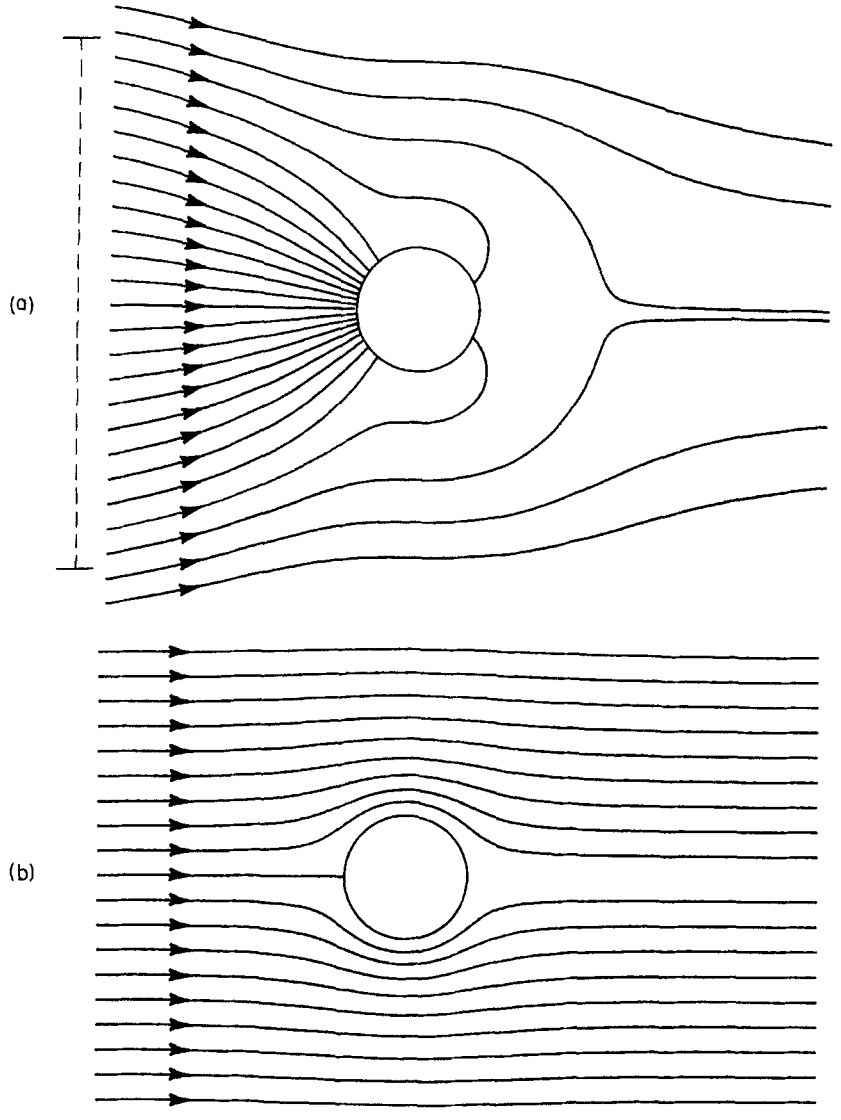

Figure 12.4 Field lines of the total Poynting vector (excluding that scattered) around a small aluminum sphere illuminated by light of energy 8.8 eV (*a*) and 5 eV (*b*). The dashed vertical line in (*a*) indicates the effective radius of the sphere for absorption of light.

expected for such a small target: a few lines intersect the sphere but most are deflected around it.

The imaginary part of the dielectric function of SiC at its Fröhlich frequency in the infrared (about 932 cm^{-1}) is close to that of aluminum at 8.8 eV. So Fig. 12.4*a* also shows the field lines of the Poynting vector around a small SiC sphere illuminated by light of frequency 932 cm^{-1}. At nearby frequencies, 900

cm^{-1} for example, the field lines around a SiC sphere ($x = 0.3$) are similar to those shown in Fig. 12.4*b* for aluminum at 5 eV.

No textbook on electromagnetic theory would be complete without a figure showing the field lines around a sphere in an electrostatic field. The reason, of course, is that this is a very effective way of presenting an idea—the sphere distorts the otherwise uniform field—in such a way that it can be grasped at a glance. But a small sphere illuminated by a plane wave also disturbs the flow of electromagnetic energy in its neighborhood. So the field lines of the Poynting vector (excluding that of the scattered field) around the sphere help to elucidate how a particle can absorb more than the light incident on it.

12.2 SURFACE MODES IN NONSPHERICAL PARTICLES

In many ways, surface modes in nonspherical particles are more interesting than those in spherical particles. Moreover, they are more likely to be observed in laboratory investigations: it is not easy to prepare samples of particles that are small compared with the wavelength, spherical to a high degree, and unagglomerated. Yet this is what is required if predictions based on the theory for small particles are to be legitimately compared with measurements. Unless special care is taken (we shall have more to say about this in the following section), solid particles prepared in the laboratory are likely to be nonspherical; even if spherical at their moment of birth, they can quickly coagulate into irregular clumps. When we leave the laboratory and seek out solid particles in natural environments—the earth's atmosphere, interplanetary space, the interstellar medium—it is almost certain that such particles are not spherical. It is often assumed that shape is irrelevant to extinction spectra of small particles: a collection of randomly oriented irregular particles is "equivalent" somehow to a collection of spheres. As we shall see, this assumption is demonstrably false in the surface mode region. Therefore, if data are analyzed, or computations are based, on the assumption that irregularly shaped particles can be adequately approximated by spheres, the results can be greatly in error.

Notable progress in analyzing nonspherical particles has been made by Fuchs (1975), who calculated absorption by cubes in the electrostatics approximation and applied the results to experimental data for MgO and NaCl. We shall discuss Fuchs's results at the end of Section 12.3. Langbein (1976) also did calculations for rectangular parallelepipeds, including cubes, which give valuable insights into nonspherical shape effects. Because the cube is a common shape of microcrystals, such as MgO and the alkali halides, these theoretical predictions have been used several times to interpret experimental data. We shall do the same for MgO. Our theoretical treatment of nonsphericity, however, is based on ellipsoids. Despite its simplicity, this method predicts correctly many of the nonspherical effects.

12.2.1 Ellipsoids

There is no "exact" theory for irregularly shaped particles; nor is there an approximate theory suitable for our purposes. Indeed, the very notion of what

precisely is an irregular particle is clouded by ambiguity; it is difficult to parameterize nonsphericity in general. Except for infinite cylinders, the exact theory for other regular shapes (e.g., spheroids and ellipsoids) is quite complicated. Fortunately, many of the interesting surface mode effects occur in particles small compared with the wavelength; therefore, we can appeal to electrostatics (i.e., the Rayleigh theory of Chapter 5) for guidance, if not for exact quantitative results. Ellipsoidal particles, which include spheres and long cylinders (needles) as special cases, represent perhaps the simplest departure from sphericity. If the incident electric field is parallel to a principal axis of a small, homogeneous ellipsoid of volume v, then its polarizability (5.32) may be written

$$\alpha = v\frac{\epsilon - \epsilon_m}{\epsilon_m + L(\epsilon - \epsilon_m)}, \tag{12.26}$$

where the geometrical factor L may take any value from 0 to 1, and we have omitted the subscript from the dielectric function ϵ of the particle for convenience. The absorption and scattering cross sections corresponding to (12.26) are

$$C_{\text{abs}} = \mathrm{k}\,\mathrm{Im}\{\alpha\}; \qquad C_{\text{sca}} = \frac{\mathrm{k}^4}{6\pi}|\alpha|^2,$$

where k is the wave number. Thus, there will be a resonance in *both* cross sections (i.e., a surface mode will be excited) at the frequency where the denominator of α vanishes:

$$\epsilon = \epsilon_m\left(1 - \frac{1}{L}\right). \tag{12.27}$$

For any real material, the frequency at which (12.27) is satisfied is complex—the surface modes are virtual. However, its real part is approximately the frequency where the cross sections have maxima, provided that the imaginary part is small compared with the real part. We shall denote this frequency by ω_s. For a sphere, ω_s is the Fröhlich frequency ω_F. If used intelligently, always keeping in mind its limitations, (12.27) is a guide to the whereabouts of peaks in extinction spectra of small ellipsoidal particles; but it will not necessarily lead to the exact frequency.

There is only one distinct geometrical factor L for a sphere; there are two for a spheroid, and three for the general ellipsoid. Thus, there is the possibility of one, two, or three distinct extinction peaks depending on the shape of the particle. The width, height, and separation of these peaks depends, of course, on the behavior of the dielectric function. Because of the wide range of $1/L$, (12.27) may be satisfied over a correspondingly wide range of frequencies; but again, this depends on the shape and magnitude of the dielectric function.

The geometrical factors for spheroids are given by (5.33) and (5.34), together with the relations $L_2 = L_3$ (prolate) or $L_1 = L_2$ (oblate) and $L_1 + L_2$

$+ L_3 = 1$. In order to show how ϵ' for spheroid resonances depends on the ratio of axis lengths, (12.27) is plotted in Fig. 12.5. For any value of L_j, a surface mode resonance will occur at the frequency where ϵ'/ϵ_m has the value given by a point on the curve. The positions of ϵ'/ϵ_m for a sphere and for several spheroids, including the limiting cases of disks and circular cylinders, are shown for different polarizations of the incident electric field. For a sphere, of course, all L_j are equal, and the resonance condition is $\epsilon'/\epsilon_m = -2$ regardless of the polarization of the incident light. The resonance condition for a prolate spheroid is split into two branches: ϵ'/ϵ_m moves down the curve toward $-\infty$ with increasing elongation for the electric field parallel to the long axis and up the curve toward -1 for the electric field perpendicular to this axis. Similarly, the resonance condition for an oblate spheroid has two branches, the end points of which are 0 and $-\infty$. There should thus be two peaks in the absorption spectrum of randomly oriented spheroids and dichroism (absorption depending on polarization) for aligned spheroids; experimental verification of this for metallic particles will be discussed in Section 12.4.

In the preceding paragraphs we discussed only the conditions for surface mode resonances in the cross sections of small ellipsoidal particles. We now turn to specific examples to further our understanding of these resonances.

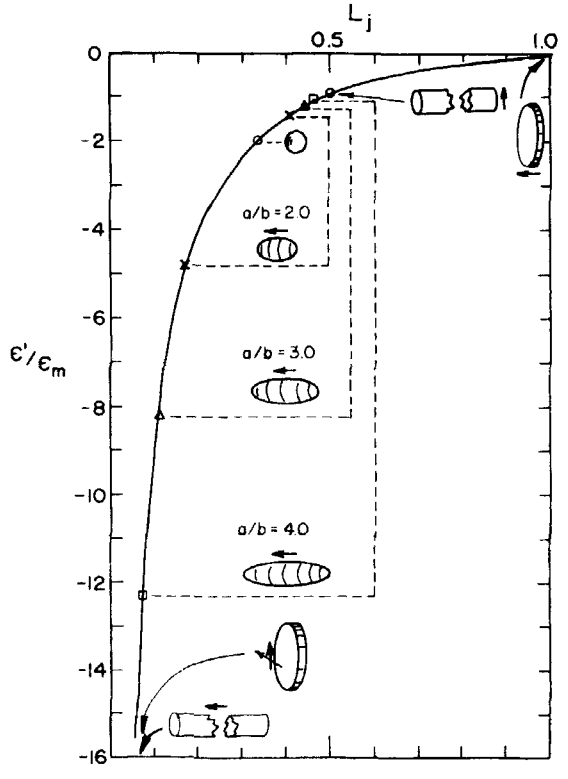

Figure 12.5 Effect of shape on the position of the lowest-order surface mode of small spheroids. Arrows next to the various shapes show the direction of the electric field.

12.2.2 Metallic Ellipsoids

In this section we try to extract as much physics as possible from a combination of electrostatics and the Drude theory of metals. It must be kept in mind, however, that our conclusions are rigorously correct only to the extent that both of these theories are valid. But by sacrificing rigor, we gain in understanding and insight.

The frequency-dependent absorption cross section of a metallic ellipsoid with dielectric function (9.26) is

$$C_{\text{abs}}(\omega) = \frac{v\gamma\omega_p^2}{c} f(\epsilon_m, L) \frac{\omega^2}{\left(\omega^2 - \omega_s^2\right)^2 + \gamma^2\omega^2}, \tag{12.28}$$

where c is the speed of light *in vacuo* and

$$\omega_s^2 = \frac{L\omega_p^2}{\epsilon_m - L(\epsilon_m - 1)}, \qquad f(\epsilon_m, L) = \frac{\epsilon_m^{3/2}}{\left[\epsilon_m - L(\epsilon_m - 1)\right]^2}.$$

By means of this combination of the cross section for an ellipsoid with the Drude dielectric function we arrive at resonance absorption where there is no comparable structure in the bulk metal absorption. The absorption cross section is a maximum at $\omega = \omega_s$ and falls to approximately one-half its maximum value at the frequencies $\omega = \omega_s \pm \gamma/2$ (provided that $\gamma^2 \ll \omega_s^2$). That is, the surface mode frequency is ω_s or, in quantum-mechanical language, the surface plasmon energy is $\hbar\omega_s$. We have assumed that the dielectric function of the surrounding medium is constant or weakly dependent on frequency.

When $L = 1$, the surface mode frequency is the plasma frequency, which for most metals lies in the ultraviolet; when $L = 0$, ω_s vanishes. So there is an enormous range of possible collective excitations in small, ellipsoidal, metallic particles: their frequencies can be anywhere from the ultraviolet to the radio. For a given shape, the surface mode frequency is a monotonically decreasing function of ϵ_m; so in going from free space to a denser medium, the surface mode frequencies shift to lower values.

The maximum absorption cross section is

$$C_{\text{abs}}(\omega_s) = \frac{v\omega_p^2}{c\gamma} f(\epsilon_m, L). \tag{12.29}$$

Note that for particles in air ($\epsilon_m = 1$), the maximum absorption is independent of shape. But if the particles are embedded in some nonvacuous medium ($\epsilon_m > 1$), the high-frequency peaks are greater than the low-frequency peaks. The maximum ratio of the height of peaks is $f(\epsilon_m, 1)/f(\epsilon_m, 0) = \epsilon_m^2$.

Up to this point we have considered only a single ellipsoidal particle oriented so that the electric field of the incident wave is parallel to one of its

principal axes. A more realistic configuration is a collection of identical particles that are randomly oriented. The average absorption cross section $\langle C_{abs} \rangle$ of such a collection is merely the arithmetic average of the three principal cross sections:

$$\langle C_{abs} \rangle = k \, \mathrm{Im}\left\{ \frac{\alpha_1 + \alpha_2 + \alpha_3}{3} \right\}, \tag{12.30}$$

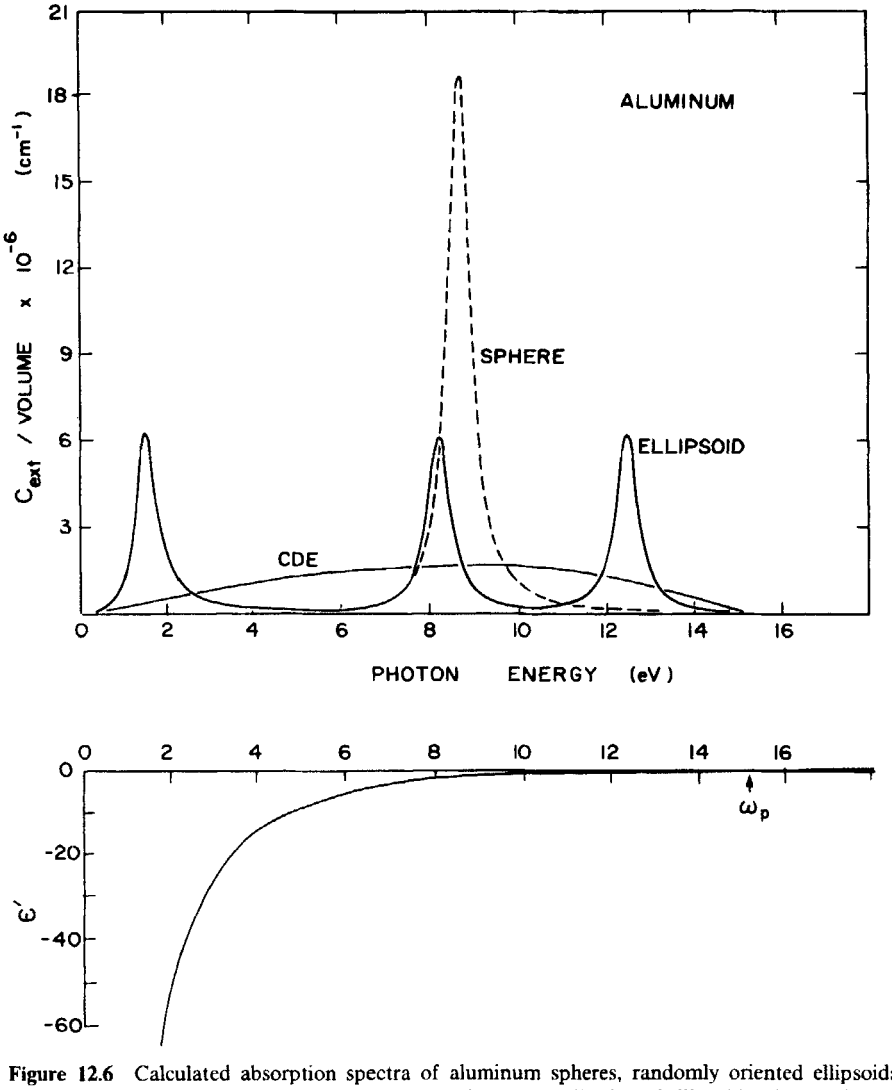

Figure 12.6 Calculated absorption spectra of aluminum spheres, randomly oriented ellipsoids (geometrical factors 0.01, 0.3, and 0.69), and a continuous distribution of ellipsoidal shapes (CDE). Below this is the real part of the Drude dielectric function.

where α_j is given by (12.26) with $L = L_j$. Thus, the absorption spectrum corresponding to (12.30) is characterized, in general, by three distinct peaks of approximately equal width (provided, of course, that the separation of surface mode frequencies is large compared with the width of the peaks). Moreover, if the particles are in air, the height of all three peaks is approximately the same. This is shown in Fig. 12.6, where the absorption spectrum of ellipsoidal aluminum particles is given. Also shown in this figure is the absorption spectrum for spheres, which has a single peak; the absorption spectrum for spheroids would exhibit two peaks. We shall explain the significance of the curve labeled CDE in a later section.

Let us return now to a single oriented ellipsoid. Integrated absorption is sometimes of interest:

$$\int_0^\infty C_{\text{abs}}(\omega)\,d\omega = \frac{v\gamma\omega_p^2}{c} f(\epsilon_m, L) \int_0^\infty \frac{\omega^2}{\left(\omega^2 - \omega_s^2\right)^2 + \gamma^2\omega^2}\,d\omega, \quad (12.31)$$

where the upper limit of integration should not be interpreted too rigidly. Obviously, the Rayleigh theory fails to be valid for indefinitely large frequencies. So the symbol infinity in (12.31) indicates a frequency sufficiently large that the absorption cross section is negligible, but not so large that Rayleigh theory is inapplicable. It may be shown by applying the residue theorem that

$$\int_0^\infty \frac{\omega^2}{\left(\omega^2 - \omega_s^2\right)^2 + \gamma^2\omega^2}\,d\omega = \frac{\pi}{2\gamma},$$

for all values of γ/ω_s; therefore, the integrated absorption is

$$\int_0^\infty C_{\text{abs}}(\omega)\,d\omega = \frac{\pi}{2}\frac{v\omega_p^2}{c} f(\epsilon_m, L). \quad (12.32)$$

There are several interesting observations that can be made about (12.32). Integrated absorption is independent of the damping constant γ; the only bulk parameter that affects it is the plasma frequency. If the particles are in air, then integrated absorption is independent of the shape; this is true not only for a single oriented ellipsoid but also for a collection of randomly oriented ellipsoids. It is instructive to rewrite (12.32) using (12.29):

$$\int_0^\infty C_{\text{abs}}(\omega)\,d\omega = \frac{\pi}{2}\gamma C_{\text{abs}}(\omega_s),$$

which shows that there is a simple proportionality between peak and integrated absorption.

12.2.3 Vibrational Surface Modes in Ellipsoids

The frequency-dependent absorption cross section of an ellipsoid with dielectric function (9.20) is

$$C_{\text{abs}}(\omega) = \frac{v\gamma\omega_p^2}{c\sqrt{\epsilon_m}} f(\xi, L) \frac{\omega^2}{\left(\omega^2 - \omega_s^2\right)^2 + \gamma^2\omega^2},$$

$$\omega_s^2 = \omega_t^2 + \frac{L\omega_p^2}{\epsilon_m + L(\epsilon_{0e} - \epsilon_m)}, \tag{12.33}$$

$$f(\xi, L) = \frac{1}{[1 + L(\xi - 1)]^2}, \qquad \xi = \frac{\epsilon_{0e}}{\epsilon_m}.$$

Equation (12.33) is similar in form to (12.28), the absorption cross section of a metallic ellipsoid: the maximum absorption is at ω_s and the half-width of the absorption peak is approximately γ. There are some important differences between absorption spectra of ionic and metallic ellipsoids, however. If we use the approximate relation (9.23), then ω_s may be written

$$\omega_s^2 = \omega_t^2 \left[\frac{\epsilon_{0v} + \epsilon_m(1/L - 1)}{\epsilon_{0e} + \epsilon_m(1/L - 1)} \right],$$

from which it follows that ω_s lies between ω_t and ω_l. This is in marked contrast with ω_s for metallic ellipsoids, which ranges from 0 to the plasma frequency. Note also that the maximum absorption cross section

$$C_{\text{abs}}(\omega_s) = \frac{v\omega_p^2}{\gamma c\sqrt{\epsilon_m}} f(\xi, L)$$

is not independent of particle shape except in the special case where $\epsilon_{0e} = \epsilon_m$. In general, the low-frequency peaks are higher than the high-frequency peaks; the maximum ratio is $f(\xi, 0)/f(\xi, 1) = \xi^2$.

The average cross section of identical, but randomly oriented ellipsoids will, in general, exhibit three peaks in the frequency range between ω_t and ω_l. An example of this is given in Fig. 12.7, where C_{abs} for a silicon carbide ellipsoid is shown as a function of frequency.

12.2.4 Randomly Oriented Disks, Needles, and Spheres

In the two preceding sections we considered features in the absorption spectra of idealized ellipsoids. Because of the simple form of the dielectric functions we

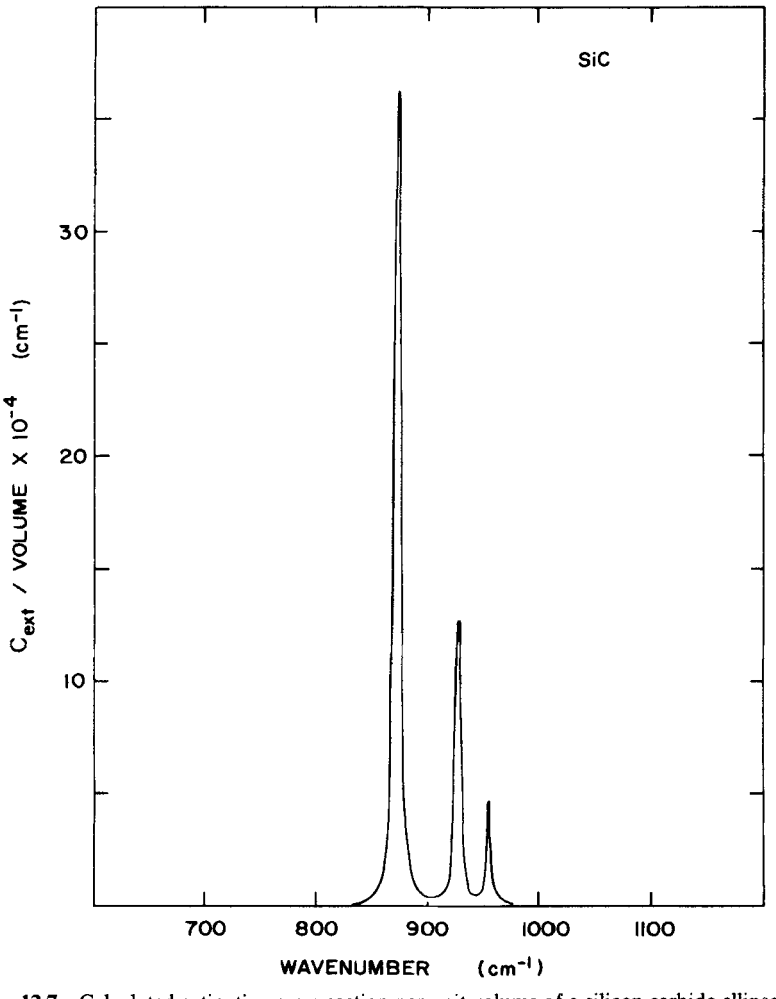

Figure 12.7 Calculated extinction cross section per unit volume of a silicon carbide ellipsoid with geometrical factors 0.1, 0.3, and 0.6. $C_{ext} \simeq C_{abs}$ for sufficiently small absorbing particles.

were able to obtain explicit expressions for the frequency-dependent cross section from which the position, width, and height of spectral features were obvious almost at a glance. But nature is not so cooperative as to provide us with only such simple materials; in general, recourse must be had to experimentally determined dielectric functions. In this section, therefore, we emphasize how the cross sections depend on the real and imaginary parts of the dielectric function, keeping in mind, of course, that these quantities are frequency dependent, but without actually specifying this dependence.

Corresponding to each point in the triangular region of the L_1L_2 plane shown in Fig. 12.8 there is a unique ellipsoid, and conversely. It would be an

unmanageable task, therefore, to consider all possible ellipsoids; but it also is hardly necessary to do so. Spheres, disks, and needles represent extreme forms of ellipsoids; they more or less bracket the range of possibilities. Moreover, they are readily visualized. So let us restrict ourselves for the moment to these three shapes. The average cross sections for identical, but randomly oriented particles are

$$\begin{aligned}
\langle C_{\text{abs}}\rangle_{\text{sphere}} &= \frac{kv}{3}\left[\frac{27}{(\epsilon'+2)^2+\epsilon''^2}\right]\epsilon'', \\
\langle C_{\text{abs}}\rangle_{\text{needle}} &= \frac{kv}{3}\left[\frac{8}{(\epsilon'+1)^2+\epsilon''^2}+1\right]\epsilon'', \\
\langle C_{\text{abs}}\rangle_{\text{disk}} &= \frac{kv}{3}\left[\frac{1}{\epsilon'^2+\epsilon''^2}+2\right]\epsilon'', \\
\langle C_{\text{sca}}\rangle_{\text{sphere}} &= \frac{k^4v^2}{18\pi}|\epsilon-1|^2\left[\frac{27}{(\epsilon'+2)^2+\epsilon''^2}\right], \\
\langle C_{\text{sca}}\rangle_{\text{needle}} &= \frac{k^4v^2}{18\pi}|\epsilon-1|^2\left[\frac{8}{(\epsilon'+1)^2+\epsilon''^2}+1\right], \\
\langle C_{\text{sca}}\rangle_{\text{disk}} &= \frac{k^4v^2}{18\pi}|\epsilon-1|^2\left[\frac{1}{\epsilon'^2+\epsilon''^2}+2\right],
\end{aligned} \tag{12.34}$$

where ϵ is the dielectric function of the particle relative to that of the surrounding medium and k is the wave number in this medium. It is clear that, at a given frequency, the only difference between the cross sections for the three shapes is the term in brackets. We are now in a position to examine further the origin of the misconception that there are no shape effects in extinction spectra of small particles. For most nicely behaved materials (insulators at visible wavelengths, for example), ϵ'' is small and ϵ' lies between 2 and 3. If $\epsilon'' \ll 1$ and $\epsilon' = 2$, for example, the cross sections are in the ratio (sphere : needle : disk) 1 : 1.12 : 1.33. So for such a material there are no strong shape effects. If, on the other hand, $|\epsilon'|$ or ϵ'' is large, then the cross section for a disk or a needle can be appreciably greater than that for a sphere. Of course, in the region where ϵ' is negative there can be strong shape effects.

More insight into shape effects in absorption spectra of small particles can be acquired from contour plots in the complex ϵ plane; lines of constant dimensionless cross section $3\langle C_{\text{abs}}\rangle/kv$ are shown in Fig. 12.9*a*, *b*, *c*. Note that the curves are symmetric about the lines $\epsilon' = -2$, $\epsilon' = -1$, and $\epsilon' = 0$ for the sphere, needle, and disk, respectively. Three points representing certain solids

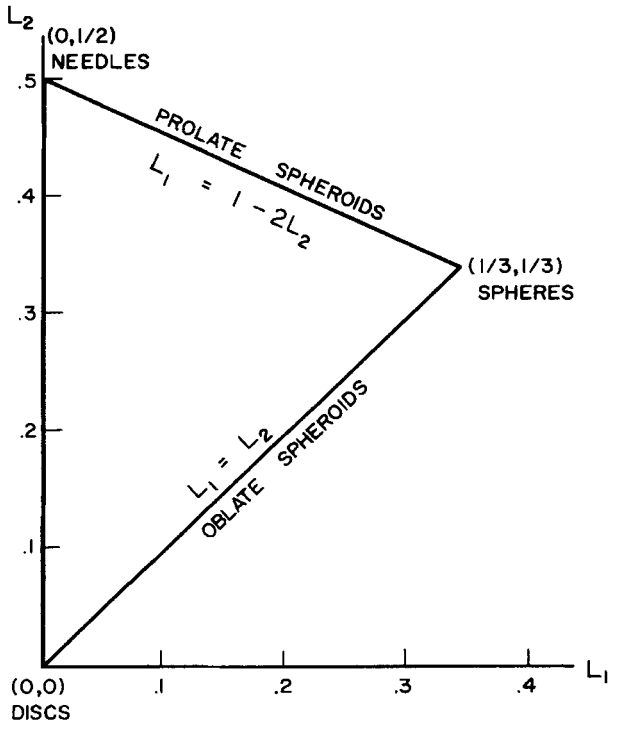

Figure 12.8 Each point of the triangular region corresponds to a unique ellipsoid, and conversely.

at specific wavelengths are labeled on the contour plots: i at $(2.3, 0.0)$ represents a typical insulator at visible wavelengths; c at $(3.0, 4.0)$ corresponds approximately to carbon in the visible; m at $(-2.0, 0.3)$ corresponds to magnesium oxide at its Fröhlich frequency (~ 620 cm^{-1}) in the infrared. Although the resolution of these contour maps is not sufficient for estimating shape effects in the vicinity of i, the calculations in the preceding paragraph indicate only slight differences ($\sim 30\%$) among the three shapes. For carbon, which is highly absorbing in the visible, estimation from the contour plots gives approximately 3, 5, and 8 for spheres, needles, and disks, respectively. But the values for MgO at its Fröhlich frequency are estimated to be greater than 50, about 3, and about 1, which shows the extreme shape dependence of small particle absorption in this instance.

Figure 12.9*d* shows the dielectric function of several metals that either have been discussed in Chapter 9 or will be discussed in connection with small particle extinction in Section 12.4. The energy dependence of the dielectric function is given in the form of trajectories in the complex ϵ plane, similar to the Cole–Cole plots (1941) that are commonly used for polar dielectrics; the numbers indicated on the trajectories are photon energies in electron volts.

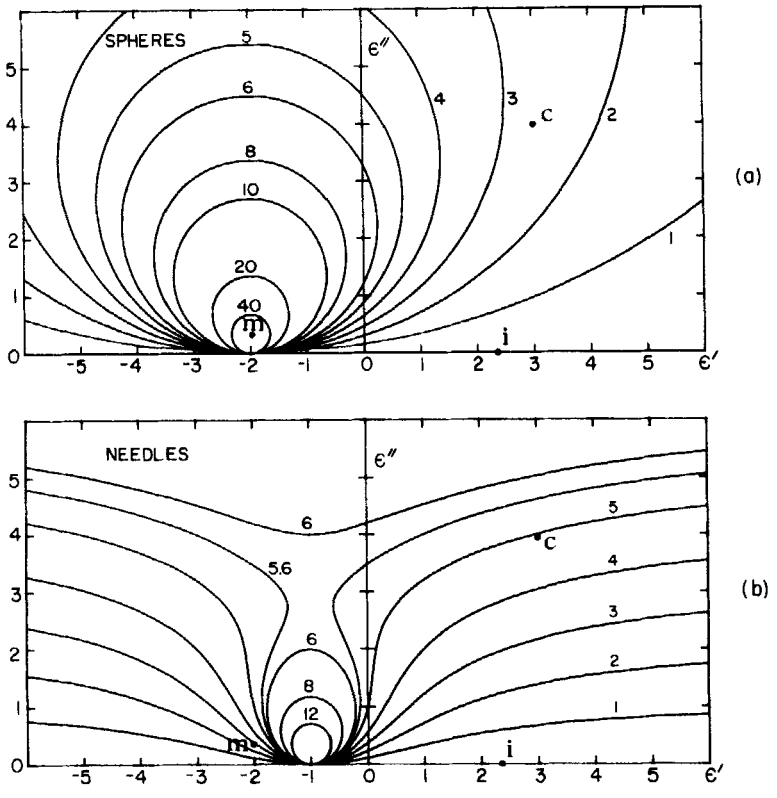

Figure 12.9 Contour plots of constant dimensionless cross section for spheres (*a*), needles (*b*), and disks (*c*). Cole–Cole plots are shown in (*d*) for various metals.

When used in conjunction with the contour plots these trajectories enable one to quickly estimate the magnitude of particle absorption and its dependence on shape. The degree to which a metal behaves like a free-electron (Drude) metal can also be determined at a glance. For example, ϵ'' of a free-electron metal goes monotonically to zero with increasing frequency as ϵ' approaches 1 from below (see Section 9.4). Aluminum is a good illustration; its trajectory is typical of a free-electron metal. From 3.0 to 3.6 eV the trajectory of silver is similar to that of aluminum, but at higher energies veers sharply from the goal of (1.0, 0.0) because of the onset of interband electronic transitions, which are discussed in connection with Fig. 9.12. The trajectory of copper nowhere looks very much like that of a Drude metal, although it terminates at the point (1.0, 0.0) as it must. Similarly, gold does not behave like a free-electron metal above 2.2 eV.

Differences in surface plasmon absorption among various metals are clearly revealed by imagining the trajectories to be superposed onto the contour plots. Spherical silver and aluminum particles have intense surface plasmon absorption peaks because ϵ'' is small at the frequency where ϵ' is -2, whereas gold

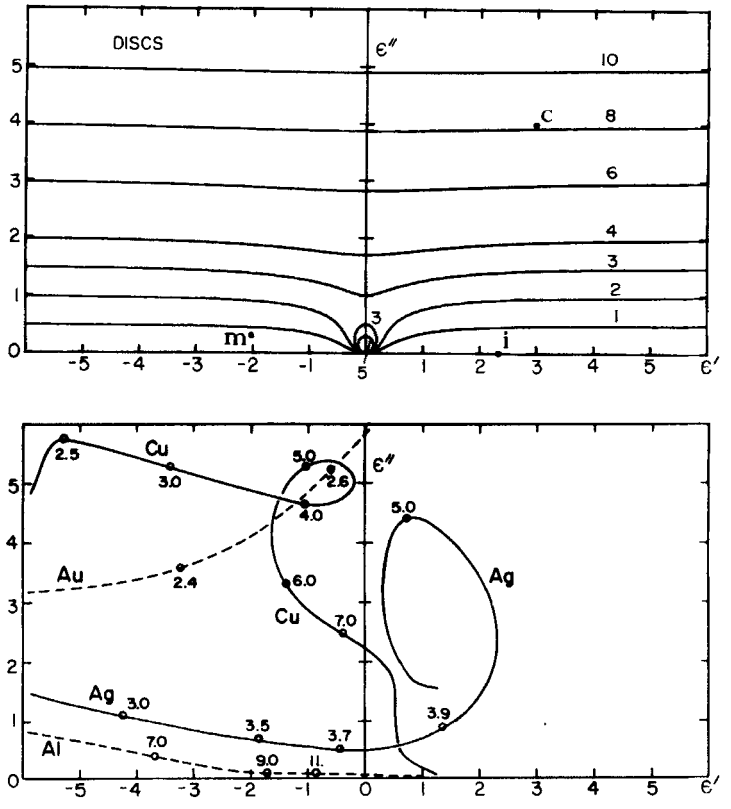

Figure 12.9 (*Continued*)

and copper particles are less absorbing because of much greater values of ϵ''. Because their trajectories closely approach the ϵ' axis, where the poles of the absorption cross section lie, absorption by silver and aluminum particles is much more dependent on shape than that by copper and gold particles.

12.2.5 Distribution of Ellipsoidal Shapes

At this point the reader who has studied the preceding sections may well wonder why we are so interested in, if not obsessed with, ellipsoidal particles: most real particles are no more ellipsoidal than they are spherical. One reason for devoting so much space to ellipsoids is that they are a means for dispelling widespread misconceptions about the nonexistence of shape effects in small-particle absorption spectra. For if there are strong shape effects in spectra of ellipsoidal particles, then there are certainly such effects in the spectra of other, less well-defined nonspherical particles. But there is at least one other reason, which may prove to be of greater practical utility: the hope that spectra of irregular particles can be approximated somehow by suitably averaging over all

ellipsoidal shape parameters to obtain simple expressions for the average absorption cross section. This idea derives from conversations with D. P. Gilra, who did calculations for distributions of spheroids. Gilra's unpublished calculations were used by Treffers and Cohen (1974) in an attempt to identify particles in the space surrounding cool stars by means of features in infrared emission spectra. In this section we derive some expressions for average cross sections under various assumptions; in later sections we shall offer experimental evidence to support the validity of these expressions in describing absorption spectra of irregular particles.

The average absorption cross section of a randomly oriented collection of *identical* homogeneous ellipsoids (12.30) may be written

$$\langle C_{\text{abs}} \rangle = \frac{kv}{3} \operatorname{Im}\left\{ \sum_{j=1}^{3} \frac{1}{\beta + L_j} \right\},$$

where $\beta = 1/(\epsilon - 1)$ and ϵ is the dielectric function of the ellipsoid relative to that of the surrounding medium. Suppose that, in addition to being randomly oriented, the collection consists of ellipsoidal particles of all possible shapes; that is, the geometrical factors L_1, L_2 are not restricted to a single set of values but are distributed according to some *shape probability function* $\mathcal{P}(L_1, L_2)$. Because of the requirement that $L_1 \leq L_2$, $\mathcal{P}(L_1, L_2)$ is strictly defined only on the hatched triangular region in the $L_1 L_2$ plane shown in Fig. 12.10. However, it is convenient to extend the domain of definition of $\mathcal{P}(L_1, L_2)$ onto the larger

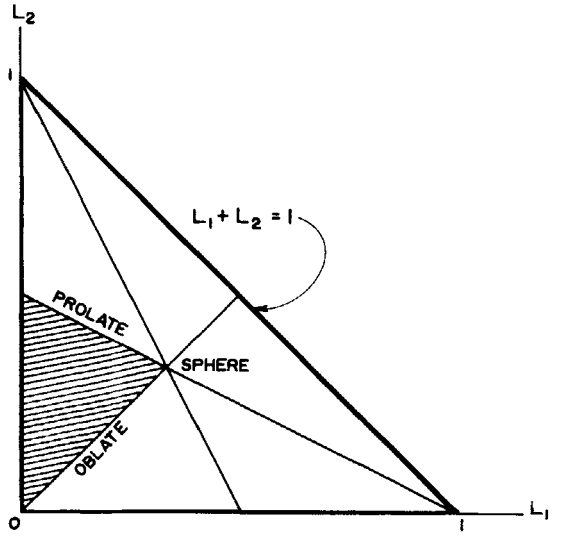

Figure 12.10 Domain of definition of the shape probability function.

triangular region Δ shown in the figure. This region may be subdivided into six equivalent regions of equal area, each of which corresponds to one of the six possible ways of choosing the relative lengths of the axes a, b, c of the ellipsoid (in Chapter 5 we required that $a > b > c$). The shape probability function is normalized to unity on Δ:

$$\iint_{\Delta} \mathcal{P}(L_1, L_2)\, dL_1\, dL_2 = 1.$$

The absorption cross section averaged over the shape distribution and over all orientations is, therefore,

$$\begin{aligned}
\langle\langle C_{\text{abs}}\rangle\rangle &= \iint_{\Delta} \langle C_{\text{abs}}\rangle \mathcal{P}(L_1, L_2)\, dL_1\, dL_2 \\
&= \frac{k v}{3} \operatorname{Im}\{\mathcal{I}_1 + \mathcal{I}_2 + \mathcal{I}_3\}, \\
\mathcal{I}_1 &= \iint_{\Delta} \frac{\mathcal{P}(L_1, L_2)}{\beta + L_1} dL_1\, dL_2, \qquad (12.35) \\
\mathcal{I}_2 &= \iint_{\Delta} \frac{\mathcal{P}(L_1, L_2)}{\beta + L_2} dL_1\, dL_2, \\
\mathcal{I}_3 &= \iint_{\Delta} \frac{\mathcal{P}(L_1, L_2)}{\beta + 1 - L_1 - L_2} dL_1\, dL_2.
\end{aligned}$$

The integral of a function $f(L_1, L_2)$ over Δ may be written as an iterated integral:

$$\iint_{\Delta} f(L_1, L_2)\, dL_1\, dL_2 = \int_0^1 dL_1 \int_0^{1-L_1} f(L_1, L_2)\, dL_2.$$

We have assumed that all particles have the same volume v; however, if there is no correlation between shape and volume, the *total* absorption cross section of the collection is

$$\mathcal{N} \frac{k\langle v\rangle}{3} \operatorname{Im}\{\mathcal{I}_1 + \mathcal{I}_2 + \mathcal{I}_3\},$$

where $\mathcal{N}$ is the total number of particles per unit volume and $\langle v\rangle$ is the average particle volume. It has also been implicitly assumed that $\mathcal{P}(L_1, L_2)$ is continuous; this is not a necessary restriction, however, and we can take into account discrete distributions by replacing the integrals above with summations over a discrete set of points (L_1, L_2) in Δ.

12.2.6 Uniform Distribution of Ellipsoidal Shapes

Perhaps the simplest conceivable distribution is one for which all shapes are equally probable, in which instance $\mathcal{P}(L_1, L_2) = 2$ and the integrals in (12.35) are readily evaluated:

$$\mathcal{G}_1 = \mathcal{G}_2 = \mathcal{G}_3 = \frac{2\epsilon}{\epsilon - 1} \operatorname{Log} \epsilon - 2.$$

Therefore, the average cross section is

$$\langle\langle C_{\text{abs}} \rangle\rangle = k v \operatorname{Im}\left\{ \frac{2\epsilon}{\epsilon - 1} \operatorname{Log} \epsilon \right\}. \tag{12.36}$$

In (12.36) Log z denotes the *principal value* of the logarithm of a complex number $z = re^{i\Theta}$ (Churchill, 1960, p. 56):

$$\operatorname{Log} z = \operatorname{Log} r + i\Theta \qquad (r > 0, \ -\pi < \Theta < \pi),$$

where Log $r = \ln r$ if r is real.

12.2.7 Summary of Shape Effects

Before presenting experimental data on surface mode absorption by small particles, we briefly summarize shape effects calculated in the Rayleigh approximation. Figure 12.11 is a schematic of surface mode absorption for the two idealized classes of solids with ϵ' negative at some frequencies: an insulator described by a one-oscillator (Lorentz) dielectric function (left) and a free-electron (Drude) metal (right); the particles are in free space. Spheres of both solids absorb strongly in the single narrow band around the frequency where ϵ' is -2; spheroids have two bands, and ellipsoids three, at frequencies determined by the relative lengths of their principal axes. Continuous distributions of ellipsoids have the broad absorption spectra sketched for both materials. Absorption bands for other nonspherical particles are expected at frequencies that depend on their shape factors (which may be laborious to calculate); for example, the six most important surface mode frequencies of an insulating cube, calculated by Fuchs (1975), are shown in the figure.

There are several important generalizations to be gleaned from this summary: (1) small particles of any shape can absorb strongly at frequencies where ϵ' is negative; (2) a distribution of shapes broadens the absorption bands at the expense of maximum absorption; and (3) although shape effects in insulating particles are confined to the region between the transverse and longitudinal optical mode frequencies, strong absorption by metallic particles may occur at any frequency from the bulk plasma frequency (commonly in the far ultraviolet) down through the visible and infrared to radio frequencies; thus, shape effects can be much more pronounced in metals than in insulators.

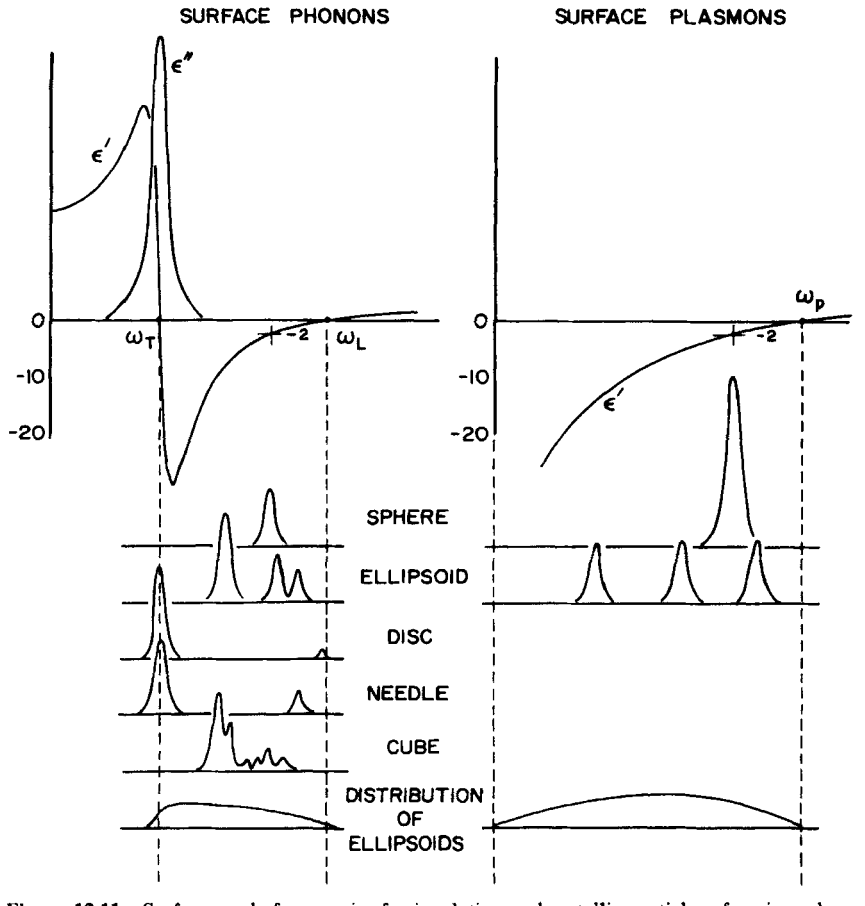

Figure 12.11 Surface mode frequencies for insulating and metallic particles of various shapes.

12.3 VIBRATIONAL MODES IN INSULATORS

In this section we compare the theory of the preceding two sections with experimental measurements of infrared extinction by small particles. Comparisons between experiment and theory for spheres of various solids, most notably alkali halides and magnesium oxide, have been published in the scientific literature; many of these papers are cited in this chapter. In most of this work, however, there is an arbitrary normalization of theory and experiment, which tends to hide discrepancies. For this reason, most theoretical calculations in this section are compared with mass-normalized extinction measurements. The new measurements presented here were made in the Department of Physics at the University of Arizona. A group of solids was selected to illustrate different aspects of surface modes. Results on amorphous quartz (SiO_2) particles, for example, illustrate the agreement between experi-

ment and theory for very small spheres described by the bulk dielectric function of the parent material. This demonstrated agreement gives confidence in the procedure of using bulk dielectric functions for small-particle calculations. Results are next shown for crystalline quartz particles, which are definitely nonspherical as well as optically anisotropic, necessitating the use of shape distribution theory and orientational averaging. Next, extinction data for SiC and MgO particles are discussed; we have used these solids for illustrative purposes in Chapters 9 and 10 and in preceding sections of this chapter. Also, there have been numerous papers relating to surface mode absorption in MgO smoke particles, which are nearly cubical in contrast with the wide distribution of shapes found in particulate samples of some of the other solids.

12.3.1 Important Experimental Considerations

For theory to be legitimately compared with experiment it is necessary that samples be prepared in which the particles are quite small (usually submicrometer), well isolated from one another, and that the total mass of particles be accurately known; also, reliable optical constants obtained from measurements on bulk samples must be at hand. These requirements are, of course, easy to state but often difficult to meet; however, if they are not met, then comparison between theory and experiment—agreement or disagreement—is likely to be specious.

In order to comply with the assumptions underlying the theory in this chapter—single, isolated, homogeneous particles—it is desirable to disperse the particles in a solid matrix. Although it might seem at first thought that dispersal in air or another gas would be more convenient and equally satisfactory, such a procedure yields a dynamic system in which the particulate characteristics continually change because of coagulation and settling. Dispersal in the zero-gravity, high-vacuum environment of an orbiting spacecraft might prevent these undesirable effects. But a considerably less expensive experimental technique is to disperse the particles in a solid matrix; this ensures that their isolation and independence are maintained. A common matrix technique, which has been used in infrared spectroscopy for many years by chemists, is the KBr pellet technique: small quantities of the particulate sample are mixed thoroughly with powdered KBr; because of the softness of KBr and its bulk transparency between about 40 and 0.2 μm, the KBr and particle mixture can be pressed into a clear pellet. Transmission measurements in conventional infrared spectrophotometers then yield extinction spectra for the particles in the KBr matrix. Although KBr has been by far the most popular matrix, other materials, such as TlBr and KI, can be used. Polyethylene powder with a dispersed particulate sample also can be pressed into infrared-transparent samples for use at wavelengths longer than about 20 μm; quite satisfactory samples can be made by pressing the powder mixture between two glass plates on a hot plate. An alternative procedure is to allow particles to collect as smoke, or by settling in air, onto thin sheets of

polyethylene film, then cut the sheets into small squares (~ 1 cm) which can be stacked and fused together between glass plates on a hot plate. A more sophisticated method, used for many years to isolate molecules and molecular clusters, is to inject the sample (vapor or particles) into a flowing gas stream of, for example, argon, which is then solidified. Martin and Schaber (1977) have used this technique in recent years to isolate small solid particles, as has Welker (1978), who also studied aggregates of silver atoms. All these matrix techniques merely serve to isolate the particles from one another and to maintain them in such a state for spectroscopic study.

The KBr technique used in most of the work reported in this section has the additional advantage that samples can be stored for many years in a desiccator without change for future study. A disadvantage is the possibility of altering some of the particles by the grinding and pressing process. To avoid this possibility some workers have opted for a loose collection of particles on an infrared-transparent substrate (see, e.g., Genzel and Martin; 1972). Although this is a perfectly acceptable approach, it usually violates our assumption of single scattering by independent particles, which thereby necessitates a modified theoretical treatment, such as the Maxwell Garnett theory, to account for the interaction between particles.

Measurements of extinction by small particles are easier to interpret and to compare with theory if the particles are segregated somehow into a population with sufficiently small sizes. The reason for this will become clear, we hope, from inspection of Fig. 12.12, where normalized cross sections using Mie theory and bulk optical constants of MgO, SiO_2, and SiC are shown as functions of radius; the normalization factor is the cross section in the Rayleigh limit. It is the *maximum* infrared cross section, the position of which can shift appreciably with radius, that is shown. The most important conclusion to be drawn from these curves is that the mass attenuation coefficient (cross section per unit particle mass) is independent of size below a radius that depends on the material (between about 0.5 and 1.0 μm for the materials considered here). This provides a strong incentive for dealing only with small particles: provided that the total particle mass is accurately measured, comparison between theory and experiment can be made without worrying about size distributions or arbitrary normalization.

There are two different ways to obtain submicrometer particles: (1) grind bulk material as finely as possible and disperse the resultant particles in air or water for segregation by settling; and (2) use a technique that generates only submicrometer particles, such as vaporization in an electric arc and subsequent condensation in a gas. Some of the particles discussed in succeeding paragraphs—amorphous SiO_2 and SiC—were prepared by arc vaporization; MgO particles were obtained by burning magnesium ribbon in air. These processes yield mostly particles that are very small (less than about 0.1 μm). Particles made from the bulk solid (quartz, for example) were ground vigorously for several hours in steel and agate mortars, dispersed both in air and in water, and settled for times long enough to leave only particles less than about 1 μm

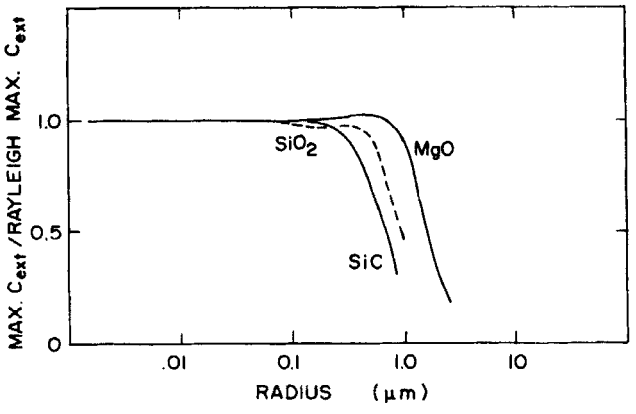

Figure 12.12 Maximum infrared extinction cross sections of spheres normalized by the value in the Rayleigh limit.

in suspension; the suspensions were then filtered to collect the particles. In all instances, about 100 μg of particles was dispersed in about 0.5 g of KBr powder. The powder–KBr mixtures were agitated in a glass vial with steel balls for periods ranging from a few hours to a few days before being pressed into pellets (~ 1 cm diameter) under a force of about 10 tons. This method of preparation seems to produce samples of particles reasonably well isolated from one another and sufficiently small that their volumetric extinction is independent of size.

12.3.2 Amorphous Quartz Spheres

A continually recurring question is the range of applicability of bulk optical constants to small particles: below what size are bulk properties no longer valid in small-particle calculations? Because *some* small-particle optical effects may be interpreted as the failure of bulk properties to be valid (see the paragraphs in Sections 12.1 and 12.4 on the limitation of the mean free path), it has become common, unfortunately, to doubt the correctness of using bulk dielectric functions even for micrometer-size particles and larger. Too often inexplicable effects exhibited by small particles—inexplicable, that is, within the framework of isolated sphere theory—are interpreted as resulting from the inapplicability of bulk properties without exploring other alternatives, such as shape effects and interactions between particles. But measurements on *nonspherical* particles cannot be compared with *sphere* calculations to decide for or against the validity of using bulk optical constants in such calculations; the only proper experimental test requires measurements on spheres. Small solid spheres are not, as a rule, easily generated; an exception is SiO_2 smoke, which can be produced readily enough by striking an arc (ac or dc) in air between silicon electrodes or carbon electrodes embedded with pieces of silicon or quartz. These smokes consist of nearly perfect spheres of amorphous SiO_2 with

diameters in the range between about 100 and 1000 Å; they satisfy the requirements of being spherical, isotropic, composed of a material with accurately measured infrared optical constants, and well within the range where volumetric extinction is independent of size. The biggest problem to be overcome is that upon formation in air the spheres link together in clusters and chains which, in electron micrographs, resemble strings of pearls. Steyer et al. (1974) published infrared extinction data on this system of particles because of its approach to ideality; however, they found a factor of 2.2 between calculated and measured peak extinction. Subsequently, experiments have been undertaken in which a more concerted effort has been made to disrupt clusters and produce isolated spheres in a KBr matrix. Results of the newer experiments are shown in Fig. 12.13, where measured extinction is compared with that calculated from sphere theory with no adjustable parameters. Bulk properties used

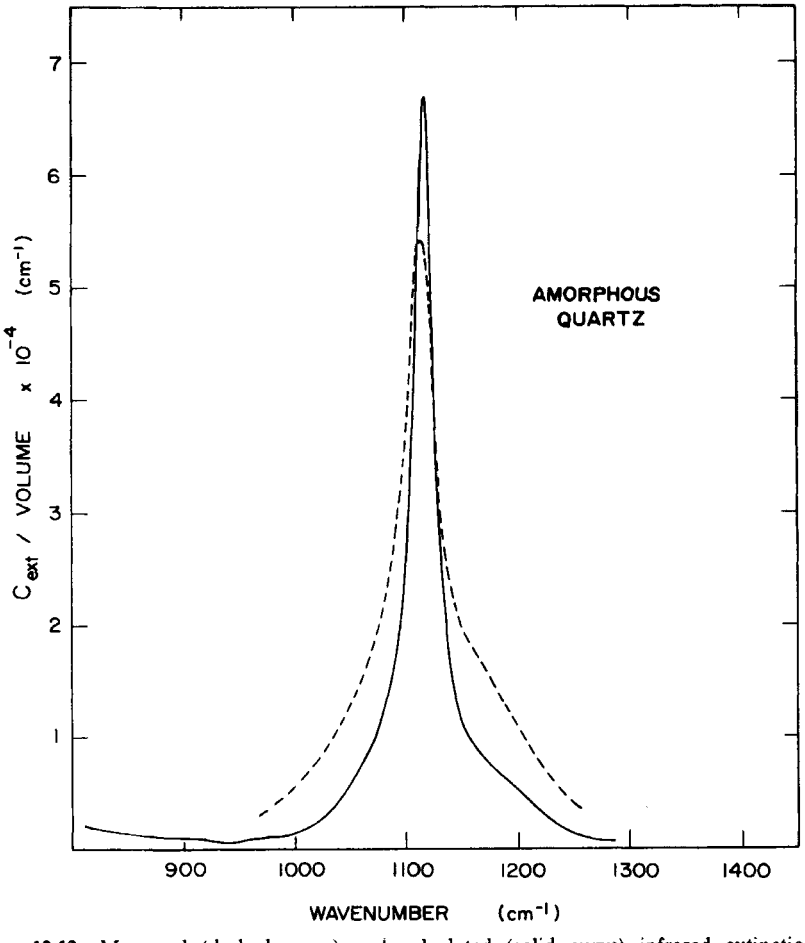

Figure 12.13 Measured (dashed curve) and calculated (solid curve) infrared extinction by amorphous quartz spheres.

in the calculations, taken from the paper by Steyer et al. (1974), agree well with independent measurements reported by Neuroth (1956) and Zolotarev (1970). Evidence that the silica spheres have been dispersed more than in earlier efforts is that the discrepancy between measured and calculated peak extinction has been reduced from a factor of 2.2 to about 20%.

Several predicted features of infrared surface mode absorption by small spheres are verified by the experimental results shown in Fig. 12.13. The frequency of peak absorption by spheres is shifted an appreciable amount from what it is in the bulk solid: the ϵ'' curve peaks at 1070 cm^{-1}, whereas the peak of the small-sphere absorption is at 1111 cm^{-1}, very close to the frequency where ϵ' is $-2\epsilon_m$ (-4.6 for a KBr matrix). The absorption maximum (absorption is nearly equal to extinction for these small particles) is very strong: Q_{abs} for a 0.1-μm particle is about 7 at the Fröhlich frequency.

We feel that the remaining discrepancy between sphere calculations and measurements can be attributed to residual clumping of particles, which causes slight broadening of the small-particle absorption bands at the expense of decreased peak height. Even without invoking such residual clumping, however, the comparison based on bulk optical constants seems favorable: the predicted absorption band—position and shape—is very close to that measured. In view of possible experimental uncertainties in the bulk dielectric function, the agreement is sufficiently close to convince us that, in this instance at least, bulk optical constants are appropriate to particles averaging considerably less than 0.1 μm in diameter.

12.3.3 Crystalline Quartz

Crystalline quartz is one of the earth's most common solid substances, bestrewing the surface as common sand. Its optical properties are anisotropic and it has strong infrared absorption bands near 9 μm. In Section 9.3, quartz exemplified an anisotropic solid the optical constants of which have been successfully extracted from infrared reflectance measurements by use of a multiple-oscillator model. Extinction measurements are presented in Fig. 12.14 for a collection of submicrometer quartz particles segregated from a finely ground powder by suspending it in water for a sufficient time to allow the larger particles to settle; these results have been published by Huffman and Bohren (1980). Comparisons of the measured volume-normalized extinction with calculations based on optical constants measured by Spitzer and Kleinman (1961) are shown in the figure. In the upper part, sphere calculations incorporating the treatment of anisotropy given in Section 5.6 are compared with measurements; without arbitrary normalization, the agreement is poor: the measured band width is much greater and the peak height much smaller than that calculated. Note that adjusting the measured and calculated curves to bring the peaks into congruence, as is commonly done, would make the agreement more favorable, but this is merely a cosmetic device that masks the discrepancies. Greatly improved agreement with experiment is exhibited by

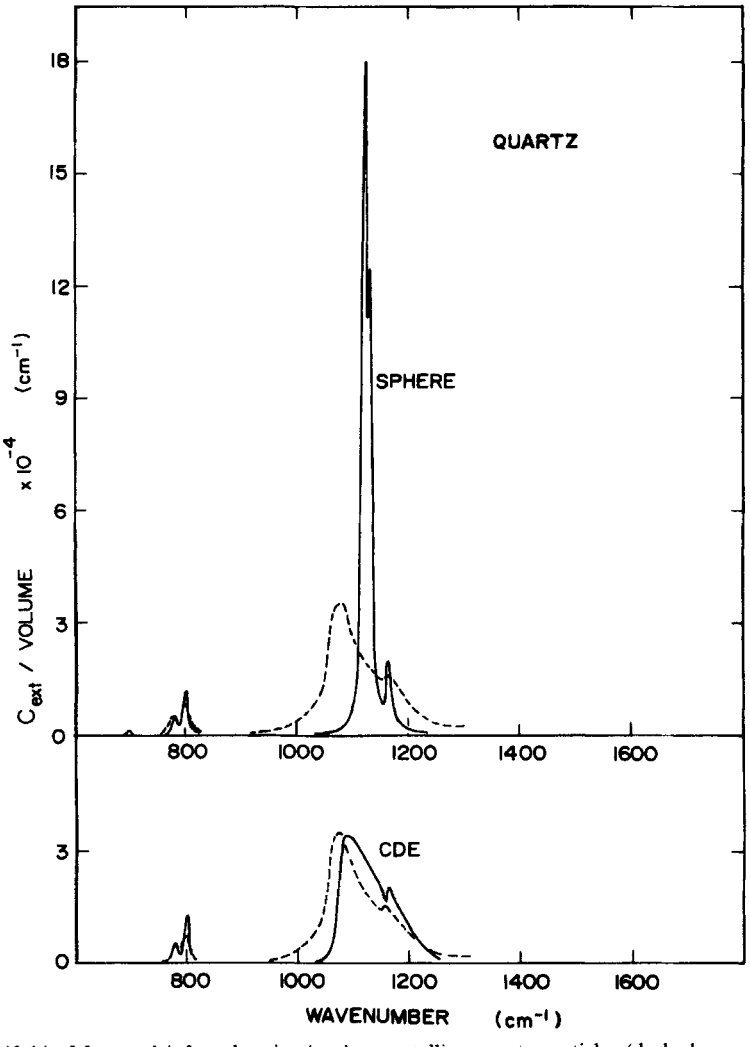

Figure 12.14 Measured infrared extinction by crystalline quartz particles (dashed curves) compared with calculations for spheres (top) and a continuous distribution of ellipsoids (bottom).

the theoretical spectrum calculated from (12.36) for a continuous distribution of ellipsoids, which is shown in the bottom part of the figure. Although all small-particle infrared spectra that we have measured have not shown such good agreement, the results do show a marked improvement in the treatment of shape effects, particularly for a sample containing particles widely distributed in shape. Moreover, the large differences between sphere calculations and those for a distribution of ellipsoids, together with good experimental agreement with the latter, bear witness to the importance of shape effects in the vicinity of strong infrared absorption bands.

12.3.4 Silicon Carbide

Although silicon carbide occurs in a variety of crystalline forms, the infrared optical properties of the major allotropes are very similar (Spitzer et al., 1959). In Section 9.1 the lattice absorption band in SiC near 11 μm was displayed as our canonical example of a real solid that conforms to a simple one-oscillator model; SiC was also invoked to illustrate surface modes in small spheres (see Figs. 12.1 and 12.2) and the effect of particle shape in the surface mode region (Fig. 12.7). Because of this prominence given to SiC we present in Fig. 12.15 experimental data for SiC particles size-segregated from powder by settling in water and then dispersed in KBr. Although we previously used the one-oscillator approximation for cubic SiC, the calculations shown in Fig. 12.15 are based on the anisotropic optical constants of hexagonal α-SiC measured by Spitzer et al. (1959). As with crystalline quartz, measurements and sphere calculations

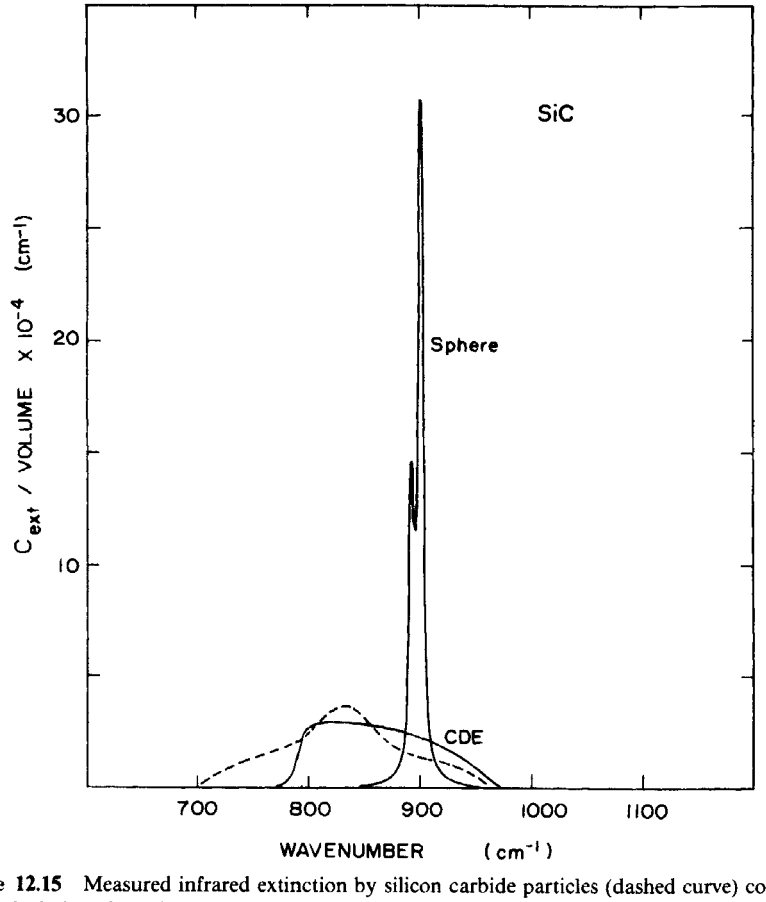

Figure 12.15 Measured infrared extinction by silicon carbide particles (dashed curve) compared with calculations for spheres and a continuous distribution of ellipsoids (CDE).

are in serious conflict. The more favorable agreement of calculations for a continuous distribution of ellipsoids (CDE) with experiment underscores the consequences of particle shape to absorption spectra. Measured integrated absorption as well as the approximate magnitude of absorption in the region between 800 and 950 cm^{-1} compare rather well with the CDE calculations. There are some discrepancies, however. Unlike the calculated band, which dips abruptly at ω_t (793 cm^{-1}), the measured absorption band extends to frequencies lower than ω_t, with just a hint of a shoulder near 780 cm^{-1}. This is the frequency region where *spheres* of SiC begin to exhibit bulk absorption modes as they depart from the behavior dictated by Rayleigh theory. These bulk modes in spheres of SiC were discussed in connection with Fig. 12.1. They would not, of course, appear in the calculations of Fig. 12.15, but they should begin to make their presence felt, although distorted in a complicated way by nonsphericity, in the larger particles (0.5–1.0 μm) of the experimental sample. Measured absorption also tends to be greater than that calculated from the CDE theory, but the peak is at a lower frequency than the sphere mode. This may be a consequence of a preferred shape among the particles, such as platelets, which would presumably not exist if the SiC particles, like the quartz particles, were ground from the bulk; the particles used in our measurements were segregated from the manufacturer's sample without further grinding because of the extreme hardness of SiC.

Further experimental evidence of shape effects in absorption spectra of SiC particles is found in the data of Pultz and Hertl (1966), who investigated infrared absorption by SiC fibers with and without SiO_2 coatings. Although these measurements were not mass-normalized, they show a strong absorption band at 795 cm^{-1} and a weaker band at 941 cm^{-1}. If the fibers are approximated as ellipsoids with $L_2 = L_3 = \frac{1}{2}$ and $L_1 = 0$ (i.e., a cylinder), then the ellipsoid equation (12.27) predicts absorption peaks for particles in air at frequencies where $\epsilon' = -1$ and $\epsilon' = -\infty$. This corresponds to absorption bands at 797 and 945 cm^{-1} for the dielectric function of isotropic SiC, in excellent agreement with the experimental peak positions for the fibers.

12.3.5 Magnesium Oxide

Possibly no other solid has been studied so much for the purpose of understanding small-particle infrared surface modes than MgO. The reason for this may in part be the ease with which small, highly crystalline cubes of MgO are generated by simply burning magnesium ribbon in air. Genzel (1974) has surveyed much of the experimental and theoretical work.

Genzel and Martin (1972, 1973) measured extinction by MgO smokes loosely packed on transparent substrates both in air and covered with the transparent oil Nujol. Their results showed absorption bands appreciably shifted from the bulk absorption band; the peak frequencies agreed with calculations, but the widths were consistently greater than predicted by sphere theory. In addition, a narrower absorption feature always appeared at the

approximate bulk absorption maximum (the maximum of ϵ''). Enhanced damping in small particles was invoked to explain the broadening. Fuchs (1975) derived an expression for absorption by cubes in the electrostatics approximation which he applied to MgO with optical constants given by a one-oscillator model, but with a damping factor larger than for bulk MgO. Fuchs (1978) has also compared results from his continuum model with the lattice-dynamical calculations of Chen et al. (1978) for an MgO microcrystal of 900 atoms ($10 \times 10 \times 9$); there was good agreement between the two theories, which suggests that relatively few atoms are necessary before an MgO particle may be properly regarded as macroscopic. Luxon et al. (1969) examined infrared absorption by several different kinds of MgO samples and, in the interpretation of their results, discussed the role of particle shape. Matumura and Cho (1981) measured emissivities in the infrared surface mode region, as did Kälin and Kneubühl (1976) for alkali halides. Despite all this effort, agreement between experiment and theory has not been completely satisfactory, particularly since arbitrary normalization is present in much of this work.

Results of our recent measurements of extinction by MgO particles are shown in Fig. 12.16. Solid curves represent experimental data, where the particles are successively more dispersed as one progresses downward; dashed curves are theoretical calculations based on the bulk optical constants measured by Jasperse et al. (1966). In the upper part of the figure volume-normalized extinction is shown for a sample prepared by burning magnesium ribbon in air and collecting the particles on a clean KBr pellet. The middle curve is for the same smoke but dispersed by grinding with KBr and shaking the mixture for 3 hours in a glass vial with steel balls before pressing a pellet; the bottom curve is for a similarly prepared sample, but shaken for 3 days before pressing a pellet.

Particles dispersed on the KBr substrate are not strictly isolated, and perhaps this should be taken into account by basing calculations on the Maxwell Garnett theory (or a similar theory) as Genzel and Martin did. The particle volume fraction is small, however, so we are not misrepresenting the experiment too badly by comparing it with calculations for isolated spheres and a continuous distribution of isolated ellipsoids. Our sphere calculations are in poor agreement with measurements, even the position of peak absorption. But Genzel and Martin obtained good theoretical agreement with measured peak absorption using the optical constants of Häfele (1963). This illustrates the sensitivity of surface mode calculations to optical constants and the consequent difficulties one often faces in deciding which among a possibly contradictory set are "best" for such calculations.

Comparison of measurements for particles dispersed *on* and *in* KBr is quite revealing. The extinction curve for particles on a KBr substrate shows a peak at approximately 400 cm^{-1}, the transverse optical mode frequency for bulk MgO. This feature has been observed a number of times and it is discussed in some of the references already cited. Its explanation now appears to be the tendency of MgO cubes to link together into chains, which more closely

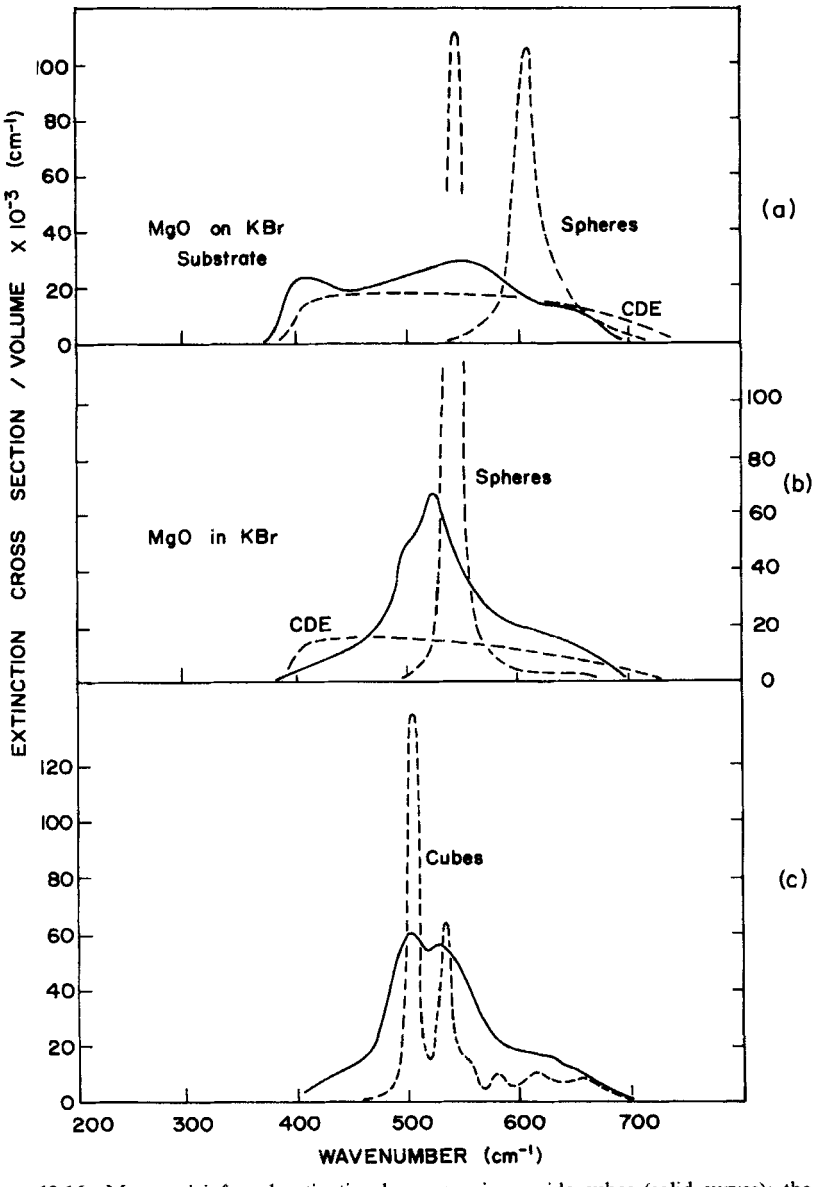

Figure 12.16 Measured infrared extinction by magnesium oxide cubes (solid curves); the particles are progressively more dispersed going from (*a*) to (*c*). Calculations for various particle shapes are shown by dashed curves.

resemble cylinders or elongated spheroids than spheres. A similar effect was observed in NiO smoke particles by Hunt et al. (1973), who analyzed their results on the basis of calculations for cylinders as well as spheres. Further evidence that the chain formation is responsible for the 400-cm^{-1} peak is that it disappears upon thorough dispersal of the particles in KBr (Fig. 12.16*b*, *c*); this was pointed out by Dayawansa and Bohren (1978).

In Fig. 12.16*b* sphere and CDE calculations are compared with measurements on MgO cubes well dispersed in KBr; neither is very satisfactory. The calculated position of peak absorption by spheres is fairly close to that measured but not coincident with it; the CDE calculations show appreciable absorption over approximately the same frequency range as the measurements but no structure. If the optical constants we have used accurately place the Fröhlich frequency, Fig. 12.16*b* suggests that neither spheres nor a broad distribution of shapes are good approximations for MgO particles. This is hardly surprising because electron micrographs reveal that MgO smoke is composed of cubes. These cubes are so nearly perfect that they have been used to quickly determine the resolution of electron microscopes: degraded resolution results in apparently rounded corners.

Fuchs's (1975) result for volume-normalized absorption by randomly oriented cubes in the electrostatics approximation is

$$k \operatorname{Im}\left\{ \sum_{j=1}^{6} \frac{C(j)}{\epsilon_m/(\epsilon - \epsilon_m) + n_j} \right\}. \tag{12.37}$$

The sum over all strength factors $C(j)$ is 1, and the n_j are analogous to the geometrical factors L_j in the expression (12.30) for the absorption cross section per unit volume of randomly oriented ellipsoids:

$$k \operatorname{Im}\left\{ \sum_{j=1}^{3} \frac{\frac{1}{3}}{\epsilon_m/(\epsilon - \epsilon_m) + L_j} \right\}.$$

We used the dielectric function ϵ of bulk MgO calculated from oscillator parameters determined by Jasperse et al. (1966), together with the dielectric function ϵ_m of the KBr matrix given by Stephens et al. (1953) (corrected by June, 1972), to calculate the absorption spectrum (12.37) of a dilute suspension of randomly oriented MgO cubes. These theoretical calculations are compared with measurements on well-dispersed MgO smoke in Fig. 12.16*c*. Superimposed on a more or less uniform background between about 400 and 700 cm^{-1}, similar to the CDE spectrum, are two peaks near 500 and 530 cm^{-1}, the frequencies of the two strongest cube modes. It appears that for the first time these two modes have been resolved experimentally. If this is indeed so we conclude that the widths of individual cube modes are not much greater than the width of the dominant bulk absorption band. Genzel and Martin (1972)

used an eightfold increase in the damping factor and Fuchs (1975) invoked a factor of 2.5 to bring theory into congruence with measurements. Such enhanced damping suggested by the broad and featureless absorption spectra previously published for MgO cubes does not seem to be necessary now in view of the apparent resolution of the cube modes. The MgO results and the agreement between theory and experiment for amorphous quartz spheres (Sections 12.3) imply that bulk optical constants do not have to be modified appreciably—by increasing the damping factor, for example—for infrared surface modes in particles in the size range 100–1000 Å.

12.4 ELECTRONIC MODES IN METALS

The first discussions of surface plasmon modes, although not designated as such, concerned colloidal silver and gold. From the classical descriptions of Faraday and the theoretical treatment of Mie to the present, the vivid colors of metal colloids have attracted serious scientific attention. In more recent years many observations have been made on surface modes in various metal and metal-like particles. These include colloidal dispersions in water, photographic emulsions and photosensitive glasses, island films formed by evaporating small quantities of metal onto smooth surfaces, cermets and granular films, aggregated color centers in alkali halide crystals, metallic smokes, electron–hole droplets in semiconductors at low temperatures, and even particles in interstellar space. Rather than survey this vast field spanning various disciplines within both pure and applied science, we have chosen a few examples that illustrate the more salient points. Gold is first, partly because of its historical interest, and because it continues to be a good example of surface mode absorption by small spherical particles at visible wavelengths. Next, silver is discussed because shape effects, which are much more pronounced in this nearly ideal free-electron metal than in gold, have been nicely demonstrated by experiment. New measurements on aluminum particles widely distributed in shape, which causes surface plasmon absorption to extend into the far infrared, is then discussed. Finally droplets of electron–hole plasma condensed in semiconductors at low temperatures are briefly treated as a modern example of surface modes in a plasma of greatly different density than common metals.

12.4.1 Gold

In his classical paper of 1908 Mie interpreted quantitatively the vivid colors of colloidal gold that had been discussed qualitatively much earlier by Faraday (1857). Despite his lack of a computer, Mie's calculations were in rather good agreement with measurements by Kirchner and Zsigmondy (1904). In recent years much theoretical and experimental work on gold particles has been published: Granqvist and Hunderi (1977) list over 50 papers published during the past 20 years. Some of this effort has been directed toward remeasuring optical constants of gold, which are (presumably) better known now than in

Mie's time. Various types of particulate systems have been studied; however, gold particles in aqueous solutions, in gelatin, and in glass are most likely to be well isolated from one another, and for this reason we emphasize these systems. To illustrate the size dependence of extinction by colloidal gold, data from Turkevich et al. (1954) and from Doremus (1964) are combined in Fig. 12.17. They investigated different size ranges, but in the region of overlap their data agree well. Because they presented their measurements differently, the curves for radii less than 26 Å are for a constant number of particles, whereas those for radii greater than 26 Å are for a constant mass. We adjusted the data of Doremus so that peak absorption is the same for the 26- and 100-Å particles. The median sizes of the larger particles studied by Turkevich et al. are the same as those for which calculations were reported by Mie (1908); they also reproduced his calculations.

The curves of Fig. 12.17 nicely illustrate the varied optical effects exhibited by small metallic particles in the surface mode region, both those explained by Mie theory with bulk optical constants and those requiring modification of the electron mean free path (see Section 12.1). Absorption by particles with radii between about 26 and 100 Å peaks near the Fröhlich frequency ($\lambda_F = 5200$ Å), which is independent of size. Absorption decreases markedly at longer

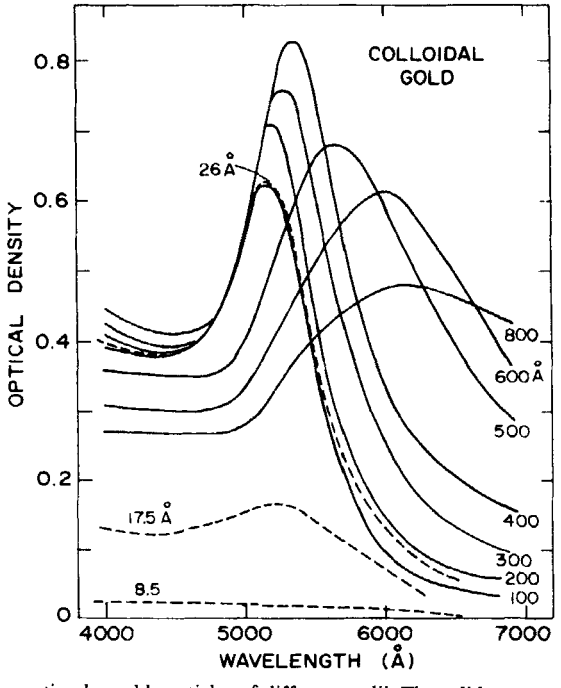

Figure 12.17 Absorption by gold particles of different radii. The solid curves are from Turkevich et al. (1954); the dashed curves are from Doremus (1964).

wavelengths (note that this is completely contrary to the absorptive behavior of thin gold films); this gives rise to the ruby red color observed in transmission of white light by small gold sols and "ruby" glass. As the radius increases beyond 100 Å the absorption peak broadens and, in accordance with (12.13), shifts to longer wavelengths; thus, the observed color changes from ruby red through purple and violet to pale blue for the largest particles (800 Å). Scattering of white light by the smaller particles is weak but becomes noticeable for particles larger than about 250 Å. The color of this scattered light is reddish brown because the scattering cross section maximum lies in the long-wavelength part of the visible spectrum; blue light by transmission is a result of both preferential scattering and absorption of longer wavelengths.

The shapes of the absorption band cease to be independent of size for particles smaller than about 26 Å, which suggests that the bulk dielectric function is inapplicable. Indeed, the broadening and lowering of the absorption peak can be explained by invoking a reduced mean free path for conduction electrons (Section 12.1). Thus, the major features of surface modes in small metallic particles are exhibited by this experimental system of nearly spherical particles well isolated from one another. But when calculations and measurements with no arbitrary normalization are compared, some disagreement remains. Measurements of Doremus on the 100-Å aqueous gold sol, which agree with those of Turkevich et al., are compared with his calculations in Fig. 12.18; the two sets of calculations are for optical constants obtained

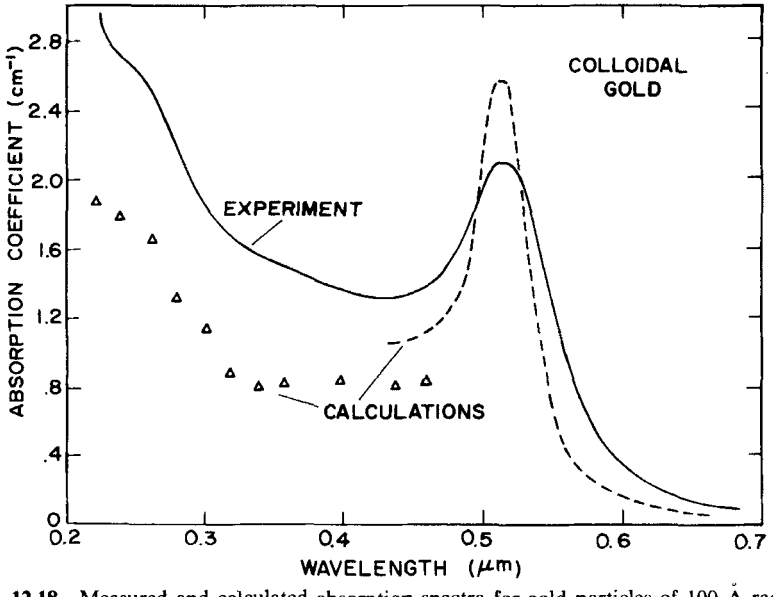

Figure 12.18 Measured and calculated absorption spectra for gold particles of 100 Å radius in aqueous suspension. From Doremus (1964).

from different sources. There is a residual discrepancy, seemingly ubiquitous: the calculated peak is sharper and higher than that measured; this was also noted by Doremus and by Granqvist and Hunderi. Doremus felt that its explanation lies in differences between bulk and small-particle absorption because of imperfections and impurities trapped by the gold particles during growth. After exploring several hypotheses, including nonsphericity and oxide coatings, Granqvist and Hunderi concluded that unavoidable clumping of particles into clusters and chains would result in effective shape factors similar to single nonspherical particles, which would broaden and decrease the absorption peak (see the summary of shape effects at the end of Section 12.2).

Despite some disagreement, it is surprising how well the combination of bulk optical constants, especially when suitably modified, and Mie theory succeeds in explaining the observed optical properties of very small particles. Doremus concluded that even without invoking mean free path limitations, the classical theory is adequate down to diameters of 85 Å; Granqvist and Hunderi found good agreement with classical calculations for particles in the size range 30–40 Å when the mean free path effect and nonsphericity are accounted for; they specifically remark that they found no evidence for a quantum size effect.

12.4.2 Silver

Surface plasmon absorption has been observed for silver particles in various media, including aqueous solutions (Kreibig, 1974), gelatin (Skillman and Berry, 1968), and glass (Stookey et al., 1978). Size effects exhibited by nearly spherical silver particles are similar to those for gold: limitation of the mean free path by the particle boundary broadens and decreases peak absorption at very small sizes, while at larger sizes the peak shifts to longer wavelengths and broadens as higher-order modes are excited. As pointed out in the discussion of Fig. 12.9, the low value of ϵ'' for silver near the Fröhlich frequency gives rise to an intense absorption band which is more sensitive to shape than the highly damped bands of gold. The Fröhlich mode for silver spheres in air is at about 3600 Å and shifts to about 4100 Å in a medium such as gelatin or glass. Because peak absorption by very small spheres occurs at the blue edge of the spectrum, increasing the size causes the transmission colors to be swept through the visible. This size effect, together with shape broadening and shifting, provides a mechanism for coloring glass (Weyl, 1951, Chaps. 24 and 25). Wiegel (1954), for example, has described colors in silver colloids ranging from yellow in the smallest sizes through the sequence red, purple-red, violet, dark blue, light blue, and gray-green as the size increases from about 100 to 1300 Å. Silver in various photosensitive materials has been widely studied because of its importance in the photographic process. This process enables particles to be generated in definite amounts by exposure and subsequently grown by photographic development. Because the number of particles remains constant as the size is increased, samples with both controlled number densities and sizes can be prepared; some control over shape has also been achieved.

Efforts to observe the effect of controlled departures from sphericity (see Section 12.2) on absorption spectra of small particles have been particularly successful for silver. Absorption spectra of three samples of silver particles produced in gelatin by photographic exposure and development are shown in Fig. 12.19 (Skillman and Berry, 1968); the average axial ratios (a/b) of the approximately spheroidal particles were determined from electron micrographs. For nearly spherical particles ($a/b = 1.18$) only one band is apparent, close to the Fröhlich mode wavelength 4200 Å; mode splitting (see the discussion of Fig. 12.5) occurs for more elongated particles ($a/b = 2.5$ and 3.35): one band moves toward longer and the other toward shorter wavelengths. The bottom half of Fig. 12.19 shows, in addition to ϵ' for silver, the two sets of wavelengths at which (12.27) is satisfied for the shape factors L_1

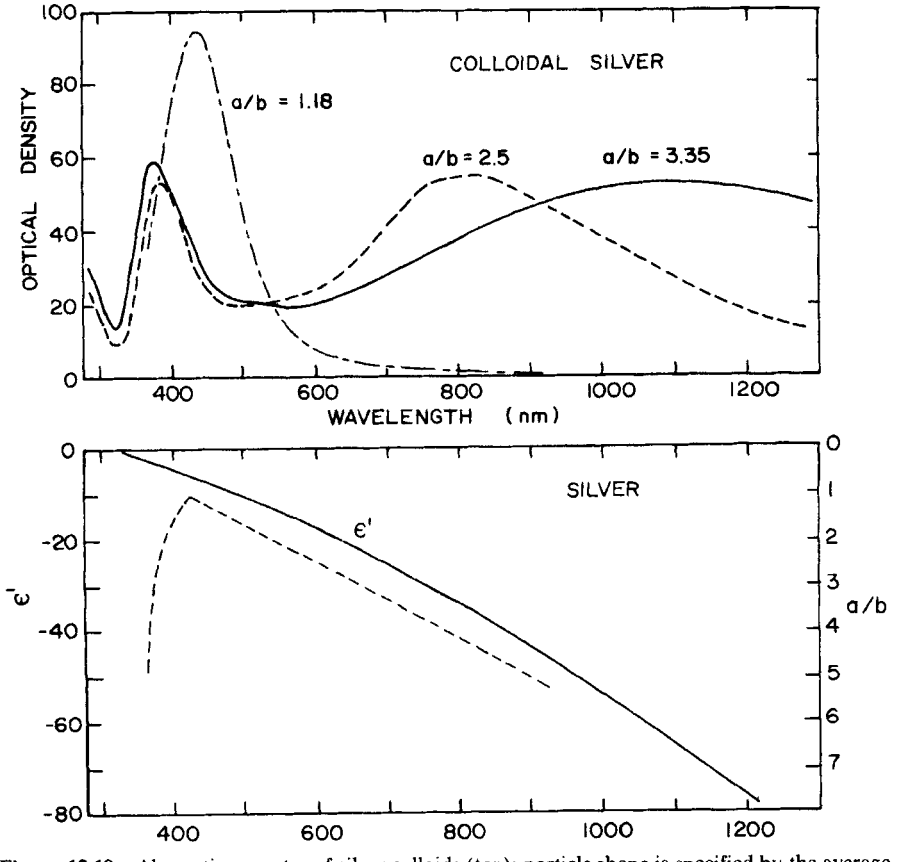

Figure 12.19 Absorption spectra of silver colloids (top); particle shape is specified by the average axial ratio a/b (from Skillman and Berry, 1968). Below this are ϵ' for silver (solid curve) and the surface mode wavelengths (dashed curves) for the two shape factors of a spheroid.

and L_2 ($L_3 = L_2$). Although there is some quantitative disagreement, measurements and calculations are qualitatively similar: the greater the particle elongation, the greater the separation of the two modes. However, the position of the short-wavelength band is predicted better than that of the long-wavelength band; this discrepancy may be the result of a distribution of spheroidal shapes, which was approximated simply by an average axial ratio, and by the fact that the particles were not perfect spheroids.

Additional measurements of absorption spectra for nonspherical silver particles were made by Stookey and Araujo (1968). Using a combination of heat treatment to grow particles in photosensitive glass and stretching to align them, they produced samples with polarization-dependent absorption; the band lies on the long-wavelength side of the Fröhlich mode if the electric vector is parallel to the long axis of the particles and on the short-wavelength side if it is perpendicular to the axis. Further experiments on photochromic glasses by Stookey et al. (1978) showed that silver is deposited selectively in the narrow tips of elongated pyramids. Although these particles are not ellipsoids, Rayleigh theory was used successfully to interpret the experimental results. However, the measured spectral shifts were somewhat *less* than those calculated, in contrast with the results of Skillman and Berry. Stookey and co-workers point out, as we did at the beginning of this section, that as a result of the low values of ϵ'' over the surface plasmon region, vitreous colloidal silver has unusually high coloring power; because of this and the possibility of spanning the visible spectrum by changing particle size and shape, various applications of this full-color photographic medium are anticipated.

Absorption resonances resulting from excitation of surface modes are accompanied by scattering resonances at approximately the same frequencies; this was pointed out following (12.26). In most experiments transmission is measured to determine extinction, which is nearly equal to absorption for sufficiently small particles. However, surface mode resonances have been observed in spectra of light *scattered* at 90° by very small particles of silver, copper, and gold produced by nucleation of vapor in an inert gas stream (Eversole and Broida, 1977). The scattering resonance peak was at 3670 Å, near the expected position of the Fröhlich mode, for the smallest silver particles. Although peak positions were predictable, differences in widths and shapes of the bands were concluded to be the result of nonsphericity.

12.4.3 Aluminum

Extinction calculations for aluminum spheres and a continuous distribution of ellipsoids (CDE) are compared in Fig. 12.6; the dielectric function was approximated by the Drude formula. The sum rule (12.32) implies that integrated absorption by an aluminum particle in air is nearly independent of its shape: a change of shape merely shifts the resonance to another frequency between 0 and 15 eV, the region over which ϵ' for aluminum is negative. Thus, a distribution of shapes causes the surface plasmon band to be broadened, the

extent of which is most apparent in extinction spectra plotted logarithmically. Figure 12.20 shows calculations, using optical constants of aluminum measured by Hagemann et al. (1974), for particles in air (solid curves) and in a medium with a dielectric function approximately equal to that of KBr over its transparent region (dashed curves). Note that there is little difference between the CDE calculations for particles in air and in a solid medium. Because the low-frequency wing of the sphere extinction spectrum is so steep, the difference between the CDE and sphere calculations becomes ever larger toward longer wavelengths: they differ by a factor of about 10^2 at 1 μm, 10^3 at 20 μm, and 10^4 at 300 μm; and at millimeter wavelengths the difference reaches 10^5. Experimental data from two sources are shown in the figure: the circles are

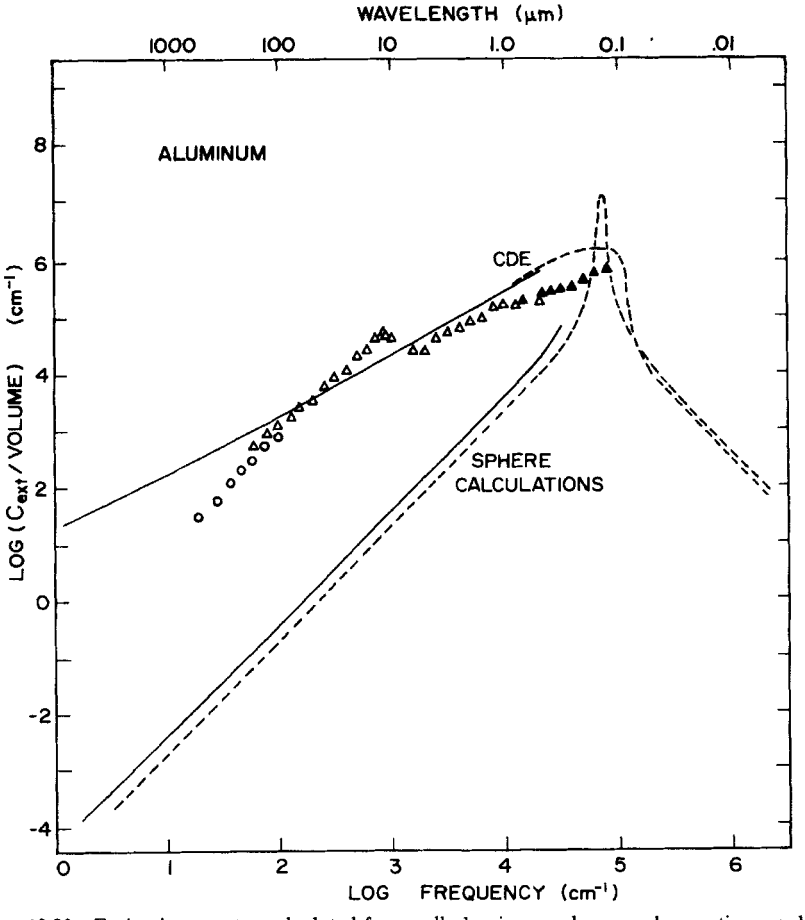

Figure 12.20 Extinction spectra calculated for small aluminum spheres and a continuous distribution of ellipsoids (CDE) in air (——) and in a medium with $\epsilon = 2.3$ (---). The circles show data from Granqvist et al. (1976), the triangles from Rathmann (1981); solid triangles are for particles on a substrate and open triangles are for particles in a matrix of KBr or polyethylene.

far-infrared measurements of Granqvist et al. (1976); the triangles are measurements of Rathmann (1981), which will be discussed shortly. Although the shape distribution of aluminum particles produced experimentally is certainly not a continuous distribution of ellipsoids, the CDE calculations are considerably closer to the data points than those for spheres; this was also true for SiC and crystalline quartz particles (Section 12.3).

The large discrepancy between sphere calculations and far-infrared extinction measurements (Fig. 12.20) has attracted much attention recently. The original impetus for such measurements was a search for superconducting band gaps of small particles. Although the telltale superconducting feature was not found, the unexpectedly high extinction inspired a series of explanations: Tanner et al. (1975) discussed the possibility of quantum size effects as the responsible mechanism; Glick and Yorke (1978) suggested a mechanism by which incomplete screening of conduction electrons near the particle surface would result in increased coupling of photons to lattice vibrations; Šimánek (1977) proposed that an amorphous oxide coating would greatly enhance absorption by particles aggregated into clusters; Maksimenko et al. (1977) and Lushnikov et al. (1978) reinvestigated the quantum-mechanical approach of Gor'kov and Eliashberg (1965) to explain the extinction; Ruppin (1979) considered both oxide coatings and spheroidal shapes incorporated into effective medium theories. Various of these ideas were reviewed and discussed at the Optical Society of America Topical Meeting on "Optical Properties Peculiar to Matter of Small Dimensions" held in Tucson, Arizona, March 1980. None of the proposed explanations seem to be completely satisfactory, particularly in view of the factor-of-10^5 discrepancy between measurements and calculations of far-infrared extinction by small platinum particles reported by Sievers.

We propose that a distribution of particle shapes broadens the surface plasmon band sufficiently that far infrared extinction is about 1000 times greater than would be obtained for spheres; this is strongly suggested by the CDE calculations of Fig. 12.20. To test this hypothesis further, extinction measurements were made over the wavelength interval between about 50 and 0.12 μm for aluminum particles prepared in a manner similar to that of Granqvist et al. (1976). Aluminum was evaporated from a tantalum boat in a helium atmosphere (~ 5 torr) and collected as very thin coatings on LiF and quartz substrates for ultraviolet, visible, and near-infrared transmission measurements. For measurements at longer wavelengths, where more mass was needed, aluminum smoke particles were dispersed in KBr and polyethylene matrices in the manner described at the beginning of Section 12.3. Volume-normalized extinction determined from transmission and mass measurements is represented by the triangles in Fig. 12.20. Agreement between measurements and calculations is considerably better for the distribution of ellipsoidal shapes than for spheres.

The peak near 18 μm is evidence for an oxide coating, which is unavoidable with the experimental technique used, on the particles. Although oxide absorp-

tion, especially in an amorphous coating on elongated particles, could give the enhanced far-infrared absorption (Šimánek, 1977), such an oxide should be weakly absorbing between about 10 and 0.3 μm. Indeed, calculated absorption by coated aluminum particles using measured optical constants of both crystalline and amorphous aluminum oxide (Rathmann, 1981) is much too low in this spectral region to account for the measurements shown in Fig. 12.20.

The considerably better agreement of CDE theory with recent measurements on aluminum smoke in the near infrared, together with similar improved agreement for nonspherical insulating particles (Section 12.3), is evidence that shape effects are indeed responsible for large far-infrared absorption by aluminum and other metallic particles. The individual particles may be highly nonspherical. But if they are nearly spherical, as they sometimes appear in electron micrographs, surface plasmon absorption would not be shifted into the far infrared; in this instance, it is likely that small clusters have not been disrupted by dispersal, which gives rise to effective shapes sufficiently different from spherical to cause the observed shifts. A similar cluster effect in gold particles on a substrate was discussed in detail by Granqvist and Hunderi (1977), who suggested this as a possibly important factor in far-infrared absorption by metallic particles.

12.4.4 Electron–Hole Droplets in Germanium

At low temperatures a pure semiconductor is a perfect insulator with no free carriers. Upon laser irradiation at a frequency greater than the semiconducting band gap, a high density of electron–hole pairs can be excited which, at liquid-helium temperatures, condense into small droplets of electron–hole plasma. These electron–hole (e–h) droplets have been discussed thoroughly in a dedicated volume of *Solid State Physics* that contains reviews of theoretical aspects (Rice, 1977) and experiments (Hensel et al., 1977).

It has been possible to measure the angular dependence of scattering by e-h droplets in germanium because the host is quite transparent between 1.66 μm (the band gap) and 25 μm (the lattice absorption band). From these measurements it was ascertained that the condensate indeed existed in the form of droplets with radii between about 1 and 10 μm.

Far-infrared absorption measurements gave an independent determination of the electron density; from the position of the Fröhlich mode near 9 meV ($\sim$ 140 μm) a density of 2.3×10^{17} cm^{-3} was inferred. Other experiments on Sb-doped Ge and pure germanium irradiated at different powers showed appreciable changes in absorption band positions and shapes. Rose et al. (1978) interpreted the shift of peak absorption from 9 meV (intrinsic Ge) to about 5.5 meV (doped Ge) as the result of an increase in droplet size under the assumption that the other e–h plasma parameters remained constant. Their (arbitrarily normalized) Mie calculations for a set of droplet sizes are shown in Fig. 12.21. There is good agreement with measurements of far-infrared absorption by e–h droplets in Sb-doped Ge (Timusk and Silin, 1975), which allows

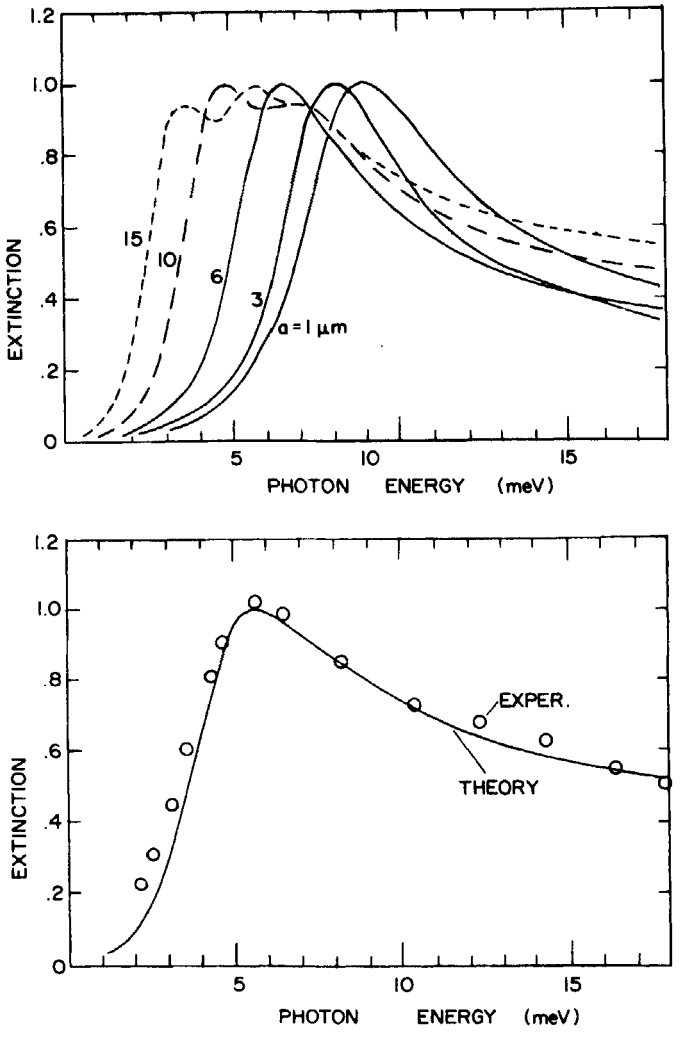

Figure 12.21 Calculated far infrared extinction (arbitrarily normalized) by electron–hole droplets in Sb-doped germanium (from Rose et al., 1978) below which are experimental data (circles) of Timusk and Silin (1975).

the droplet size to be determined where light scattering measurements are difficult because of impurity-induced opacity of the germanium host. Thus, the sizing of e–h droplets is a simple application of Mie theory coupled with Drude theory to a somewhat exotic particulate medium.

12.4.5 Survey of Other Plasmons

Surface plasmon absorption has been observed for small particles of several other metals, and many calculations have been published; these are too

numerous to discuss in detail. But it is worthwhile to summarize the properties of surface plasmons for various metallic particles. In Table 12.1 the most important parameters characterizing surface plasmons are listed: the position of the Fröhlich mode for spheres in air; and the value of ϵ'' at the frequency where $\epsilon' = -2$, which determines the width and height of the absorption band. Also listed are energies where $\epsilon' = 0$ (bulk plasmon energies) to show the possible high-energy extent of shape effects. The sources of this experimental data are indicated in the table.

The alkali metals, with only one free electron per atom, have lower plasmon energies than those of divalent free-electron metals such as Mg and Al because the plasma frequency decreases with decreasing electron density. Thus, surface plasmon energies for alkali metals are in or near the visible, whereas they are in the far ultraviolet for Mg, Al, and Pb. Surface plasmon energies of the divalent metals Ag, Au, and Cu are shifted toward and into the visible because of interband transitions (see Fig. 12.9*d*); this is also the cause of the large values of ϵ'' for Au and Cu.

Another example listed in the table is graphite, the Fröhlich mode of which is near 5.5 eV (2200 Å); the boundaries of the negative ϵ' region are about 4 and 6.5 eV. The graphite surface plasmon has been tentatively identified as responsible for a feature in the interstellar extinction spectrum (see Section 14.5).

For photon energies large compared with the band gap in semiconductors, electronic transitions are only slightly perturbed by the presence of the gap; the valence electrons in this instance act like free electrons. Thus, the high-energy optical properties of semiconductors are similar to those of free-electron metals. But there are marked differences in their low-energy optical properties, which bear on the importance of particle shape to extinction spectra. Whereas ϵ' for metals approaches large negative values with decreasing photon energy,

Table 12.1 Characteristics of Bulk and Surface Plasmons

Solid	Bulk Plasmon Energy (eV)	Surface Plasmon Energy (eV)	ϵ'' where $\epsilon' = -2$	Reference
Lithium	6.6	3.4	1.0	Rasigni and Rasigni (1977)
Sodium	5.4	3.3	0.12	Palmer and Schnatterly (1971)
Potassium	3.8	2.4	0.13	Palmer and Schnatterly (1971)
Magnesium	10.7	6.3	0.5	Hagemann et al. (1974)
Aluminum	15.1	8.8	0.2	Hagemann et al. (1974)
Iron	10.3	5.0	5.1	Moravec et al. (1976)
Copper	—	3.5	4.9	Hagemann et al. (1974)
Silver	3.8	3.5	0.28	Huebner et al. (1964)
Gold	—	2.5	5.0	Hagemann et al. (1974)
Graphite	—	5.5	2.7	Taft and Phillip (1965)

ϵ' for semiconductors becomes positive again; at photon energies below the band gap energy the optical properties of semiconductors are similar to those of insulators. Thus, the surface plasmon region—where ϵ' is negative—for semiconducting particles is bounded from above *and* from below; this contrasts with aluminum particles, for example, in which, depending on their shape, surface plasmons are possible at all energies below the plasma frequency. Consequently, shape effects in metallic particles are, in general, more pronounced than in semiconducting particles.

NOTES AND COMMENTS

Gilra (1972ab) has very thoroughly discussed absorption by small ellipsoidal particles, including those with coatings, in the surface mode region.

The question of which shape maximizes and which minimizes the absorption cross section of a particle with fixed volume and composition has been answered by Bohren and Huffman (1981) within the framework of the Rayleigh ellipsoid theory.

An independent derivation of (12.36), preceding ours, was published by Aronson and Emslie (1975).